9950-631

GEOCHEMICAL AND SPECTRAL CHARACTERIZATION OF NATURALLY ALTERED ROCK SURFACES

FINAL REPORT

for

Contract No. 955757 between

California Institute of Technology,
Jet Propulsion Laboratory

and

University of Maryland
(Subcontract under NASA Contract NAS 7-100
Task Order No. RD-151)

Luke L. Y. Chang, Principal Investigator

Sheldon E. Sommer, Previous Principal Investigator

William F. Buckingham, Graduate Research Assistant

12/23/81

TABLE OF CONTENTS

LIST OF TABLES

LIST OF FIGURES

GLOSSARY OF GEOLOGIC TERMS

aluminosilicate -- A mineral containing aluminum and silicon as the major cations.

alunite -- A white/pink hexagonal mineral usually formed by sulfuric acid reacting with potassium feldspar. Formula: $KAl_3(OH)_6(SO_4)_2$

corundum -- Hexagonal aluminum oxide. Formula: α-Al_2O_3

diaspore -- Orthorhombic aluminum oxyhydroxide. Formula: α-AlOOH

goethite -- Orthorhombic ferric oxyhydroxide. Formula: α-FeOOH

gossan -- A leached, residual mineral assemblage occurring above a zone of alteration. Formed by the weathering of sulfides, it is characterized by an orange ferric oxide color.

granodiorite -- A coarse grained igneous rock consisting chiefly of feldspar and quartz. Over 50% of the feldspar is plagioclase.

hematite -- Hexagonal ferric oxide. Formula: α-Fe_2O_3.

hydrothermal alteration -- The chemical attack on a host rock caused by the emplacement of ore minerals from an aqueous solution which emanated from a magma body.

illite -- A general term for mica-like clay minerals.

jarosite -- An orange, hexagonal, ferric hydroxide sulfate which often occurs as a secondary mineral in altered rocks. Formula: $KFe_3(OH)_6(SO_4)_2$.

kaolinite -- A clay mineral. Formula: $Al_4(Si_4O_{10})(OH)_8$.

metasediment -- A former sedimentary rock (such as limestone, shale or sandstone) which has undergone metamorphism.

montmorillonite -- A clay mineral with a variable cation composition and which has the ability to absorb water and expand.

paleosoil -- A former soil which has been buried, often by volcanic debris.

quartz monzonite -- A rock similar to granodiorite in composition but containing less quartz.

tuff -- A rock composed of fine particles of volcanic ash and dust.

INTRODUCTION

Statement of Problem

Remote sensing is the collection of information about an object without physically sampling the object. In the present study, remote sensing is restricted to the collection of visible-near infrared (400 - 2500 nm) solar radiation reflected from the earth's surface.

Visible-near IR remote sensing has been used in geology for a number of problems, notably structural analysis and topographic mapping. This study examines the possibility of using this spectral region for compositional analysis. This would allow mapping of rock type both on the earth's surface and on other planetary surfaces.

The possible use of remote sensing to map ore bodies has been explored for several years. The weathering of epithermal ore deposits produces a surface leached zone overlying the ore. The production of the leached zone and the chemical attack on the surrounding host rock is referred to as hydrothermal alteration. The leached zone, also called a gossan, often contains a unique mineral assemblage. This assemblage, formed in zones surrounding the ore body, contains high concentrations of iron oxides and oxyhydroxides, clay and other hydroxyl bearing minerals, and sulfates. Figure 1 is a photograph of an altered zone located southeast of Hawthorne, Nevada along the Walker Lane fault. The alteration occurs along a horizontal band through the center of the photo. The iron oxides give the gossan its charac-

ORIGINAL PAGE
BLACK AND WHITE PHOTOGRAPH

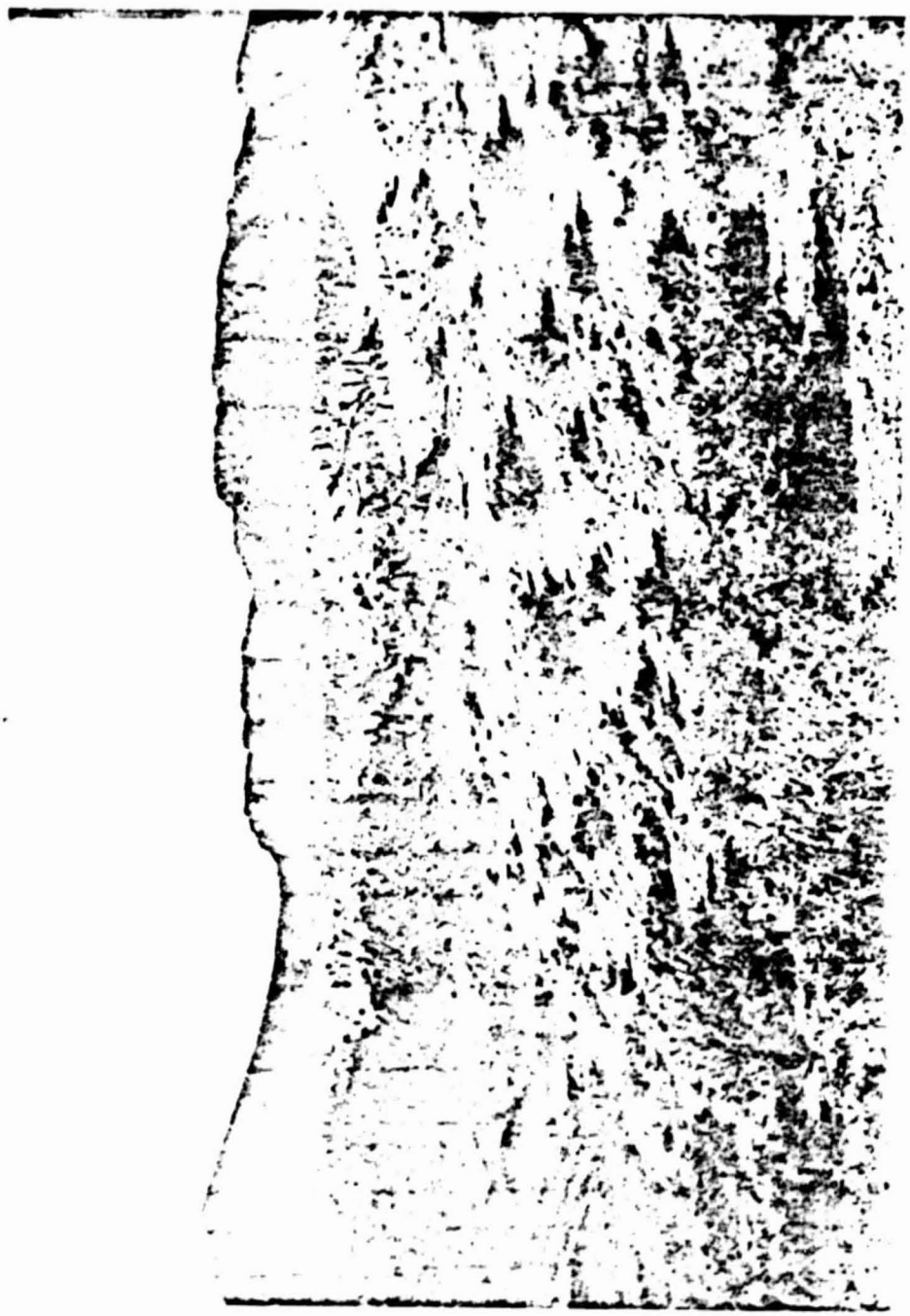

Figure 1. Photograph of hydrothermally altered region along the Walker Lane Fault southeast of Hawthorne, Nevada.

teristic red color. Clays, sulfates, and iron oxides produce absorption features in the visible-near IR. The absorption features are exhibited as spectral regions of low reflectance. Using reflectance spectroscopy, it should be possible to delineate surface regions containing these assemblages.

Early attempts to map hydrothermal alteration in this manner began with the launch of ERTS-1, the first of the Landsat satellites, in the early 1970's. Landsat was equipped with four bands in the visible-near IR. Iron oxides have absorption features within two of these bands. High ferric iron concentrations should produce low reflectance values in these bands. It was found that high iron concentrations did not always coincide with hydrothermal alteration. Other sensors were also used in airborne experiments. These sensors contained bands near 2200 nm, along with the same bands as used in Landsat. Since hydroxyl bearing minerals absorb near 2200 nm, the newer sensors could locate areas of high clay content and high ferric iron content. Because other rock types also contained clays and iron oxides, additional means are needed to distinguish altered rocks in some areas. Figure 2 is a photograph of an unaltered, iron-stained tuff located near Coaldale, Nevada. This unit contains a small concentration of hydroxyl-bearing minerals and would be misclassified as hydrothermally altered.

ORIGINAL PAGE
BLACK AND WHITE PHOTOGRAPH

Figure 3. Photograph of unaltered, broadband data
located near Coaldale, Nevada.

The problem examined in this study is the examination of hydrothermally altered rock and the visible-near IR spectral features associated with this rock. The problem is divided into three parts:

1. What are the mineralogical constituents present in the surface coatings of altered and unaltered rocks?
2. Is there a difference between the coatings formed on hydrothermally altered rocks and those formed on unaltered, weathered rocks?
3. If a difference exists between the coatings on altered and unaltered samples, can this difference be remotely sensed either through presently utilized spectral regions, or through presently unused atmospheric windows?

The Approach

Answering the questions posed in the preceding section required the mineralogical characterization of hydrothermally altered and unaltered rocks. Preceding the characterization, another question had to be dealt with. How much of a rock is sampled in reflectance spectroscopy? The remote sensing devices used collected reflected visible-near IR radiation from rocks and soils. If compositional data were to be related to the reflectance signal, then only the portion of rock or soil which contributes to the reflectance signal should be compositionally analyzed.

Synthetic samples were used to model natural rock surfaces, both compositionally and texturally. The thickness

of the synthetic samples was measurable. The relationship between the sample's thickness and reflectance was observed and the depth of penetration of visible-near IR radiation was measured.

Rocks and soils were collected along a number of western Nevada flight lines which had been flown using several remote sensing devices. Western Nevada was chosen due to the occurrence of a number of known mineralized zones, the lack of vegetation, and the generally poor soil development. The use of photographs taken during the overflights allowed collection of samples which had contributed to the reflectance signals received by the remote sensing radiometer.

In situ reflectance and laboratory visible-near IR reflectance spectra were collected from the samples. The upper 50 μm of each rock sample was characterized by several techniques, including x-ray diffraction, x-ray fluorescence, Mossbauer spectroscopy, microprobe analysis, ESCA, chemical extractions, and electron microscopy. The examination of the data collected by these techniques would note if differences existed between altered and unaltered rock. The examination of the laboratory reflectance spectra would show if mineralogical differences produced reflectance spectral features. The sample compositional data could also be related to the remote sensing data collected from the same sites. This would allow examination of the ability of remote

sensing devices to discriminate hydrothermally altered rock from the unaltered surrounding rock.

LITERATURE REVIEW

Remote Sensing

Over the past several years, remote sensing has proven to be a valuable tool in geology. The earth scientist has used photographs and imagery to delineate faults and lineament patterns (Raines, et al., 1978; Stewart, et al. 1979), observe the structure and composition of the planets (Singer, et al., 1979; Clark and McCord, 1980), construct topographic and geologic maps, and observe features too large to observe on the ground (Rowan, 1975). Several reviews of the varied uses of remote sensing in geology exist, such as Sabins (1978), Reeves (1975), and Goetz and Rowan (1981).

Remote sensing, in its broadest sense, is the collection of information about an object without contacting or sampling the object. A signal from the object or target is measured by an instrument system. The signal was produced by emission, reflection, or some other energy-matter interaction. The energy source may be the sun, in which case the remote sensing system is defined as passive. The energy source may be mounted on the sensing system, for example a laser or radar source, in which case the system is defined as active. In all cases, the sensor does not contact the target and is therefore termed a remote sensor. Throughout this study, remote sensing will be restricted to the collection and analysis of solar radiation reflected from the

earth's surface. The range of energy available for this type of information gathering is limited by the output of the sun and the ability of certain broad bands to pass relatively unhindered through the atmosphere. A variety of atmospheric constituents absorb specific segments of the incident solar radiation (figure 3). The segments between those absorbed by the atmospheric constituents are described as atmospheric windows. The energy of these regions is free to interact with the earth's surface and pass through the atmosphere to be collected by the remote sensor. The atmospheric windows occurring in the visible-near infrared portion of the spectrum (400 nm - 2500 nm) are of interest in the present study.

The visible-near infrared (VNIR) atmospheric windows have been utilized by a number of remote sensing devices for geologic research. The devices are commonly an array of detectors, each detector fitted with a band pass filter which restricts the range of energy it can detect. The total radiance (L) collected by a detector is composed of three parts:

$$L = L_s + L_a + L_r$$

where L_s is the solar radiation scattered from the atmosphere back to the detector, L_a is the solar radiation which strikes a target on the earth's surface and is reflected toward the detector, and L_r is the scattered radiation which

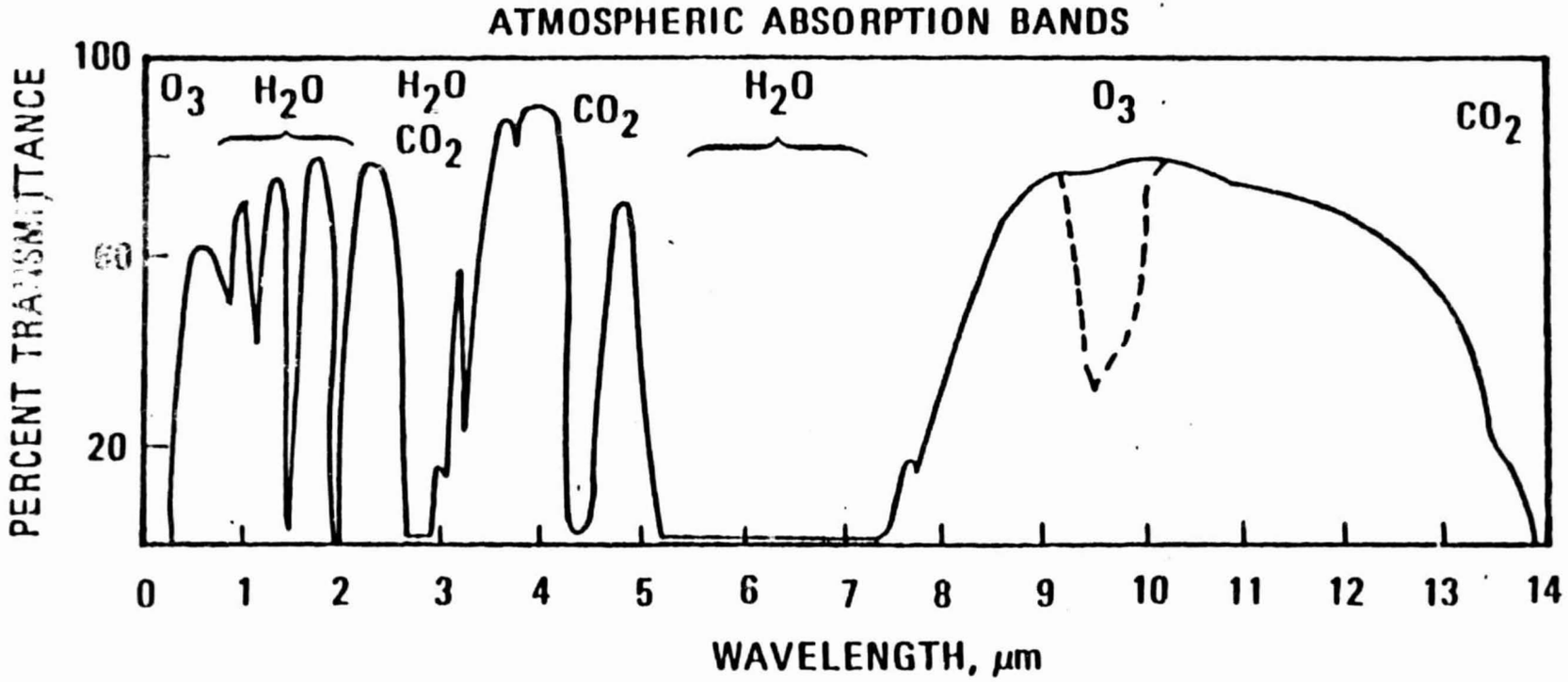

Figure 3. Atmospheric windows. Spectral regions of high transmittance are atmospheric windows. Atmospheric constituents responsible for absorption are noted. From Sabins (1978).

strikes the target and is reflected to the detector (Reeves, 1975).

Evaluating the three components over the wavelength region passing through the band pass filter yields:

$$Ls = \frac{\sin\beta}{\pi} \int_{\lambda_1}^{\lambda_2} E(\lambda)\ T_\beta(\lambda)\ T_z(\lambda)\ \rho(\lambda)\ R(\lambda)\ \delta\lambda$$

$$L_a = \frac{1}{\pi} \int_{\lambda_1}^{\lambda_2} E(\lambda)\ \rho_\beta^1(\lambda)\ R(\lambda)\ \delta\lambda$$

$$L_1 = \int_{\lambda_1}^{\lambda_2} S_z(\lambda)\ R(\lambda)\ \delta(\lambda)$$

Summing the three terms yields an expression for the total radiance striking a detector:

$$L = Ls = \frac{\sin\beta}{\pi} \int_{\lambda_1}^{\lambda_2} E(\lambda)\ T_\beta(\lambda)\ T_z(\lambda)\ \rho(\lambda)\ R(\lambda)\ \delta\lambda$$

$$+ L_a = \frac{1}{\pi} \int_{\lambda_1}^{\lambda_2} E(\lambda)\ \rho_\beta^1(\lambda)\ R(\lambda)\ \delta\lambda$$

$$+ L_r = \int_{\lambda_1}^{\lambda_2} S_z(\lambda)\ R(\lambda)\ \delta(\lambda)$$

β = solar elevation angle

$E(\lambda)$ = spectral solar irradiance at the top of the atmosphere at normal incidence

$T_\beta(\lambda)$ = monochromatic one-way transmissivity of the atmosphere at elevation angle β

$T_z(\lambda)$ = monochromatic transmissivity of the atmosphere in the zenith direction for solar radiation reflected by the surface to the nadir viewing sensor

$\rho(\lambda)$ = reflectance; the ratio between the incident and reflected electromagnetic radiation

$\rho_\beta^1(\lambda)$ = atmospheric reflectance

$R(\lambda)$ = spectral response of the sensor

$S_z(\lambda)$ = radiation scattered into the path of the sensor

Several assumptions have been made in order to apply this expression in remote sensing. L_a has been considered to be constant within a scene if viewing angle and lighting are constant. L_r may be evaluated by measuring the radiance of an object, such as a cloud shadow, which is receiving no direct incident solar radiation (Rowan, et al., 1977). L_s contains several variables, $E(\lambda)$, $T_b(\lambda)$, $T_z(\lambda)$, $R(\lambda)$ which are constant for a particular area when viewed for a short time period. The last term, $\rho(\lambda)$, contains the compositional data which may be derived from a remote sensing device.

Reflectance Spectroscopy

Reflectance is defined as the ratio of incident radiation to the reflected radiation. There are two components which comprise the reflected radiation: the specular component and the diffuse component.

Specular reflectance (R_s) is mirror-like reflection in which the radiation is reflected without penetrating the material's surface. R_s is governed by the Fresnel equation:

$$Rs = \frac{(n-1)^2 + n^2k^2}{(n+1)^2 + n^2k^2}$$

where: n = index of refraction

$$k = \frac{\alpha\lambda}{4}$$

α = absorption coefficient (Kortum, 1963; Wendlandt and Hecht, 1971)

Diffuse reflectance (R_d) is the resulting reflection when light penetrates the surface of a material, scatters within the material and between particulate surfaces, and exits the material. Diffuse reflectance is described by the Kubelka-Munk equation:

$$R_d = \frac{1 - \frac{\alpha}{\alpha + 2s}}{1 + \frac{\alpha}{\alpha + 2s}}$$

where s = scattering coefficient (Kortum, 1968)

The relative values of the two components will change as wavelength, incident angle, particle size and composition changes (Vincent and Hunt, 1968).

In the visible-near IR region, much of the incident radiation is multiply scattered and some of the radiation enters the target material where certain wavelenghts are preferentially absorbed. The major features recorded in a reflectance spectrum are produced by absorption processes (Hunt, 1980). The major absorption processes may be divided into electronic and vibrational transitions.

The electronic transitions include charge transfer bands and crystal field transition bands. The transitions involving ferric iron, a d^5 metal, are of interest in this study. Most of the vibrational features in this spectral

region are related to M-O-H vibrational overtones, where M = Al or Mg.

Economic Geology

The application of remote sensing to map mineralized zones requires the zones to contain mineral assemblages having a distinctive set of spectral features available in an atmospheric window for satellite detection. The features must be different from those associated with unmineralized zones. The ore minerals themselves must have distinctive features and be exposed on the earth's surface, or the geologic processes involved in ore emplacement must produce unique mineral assemblages.

The injection of low temperature fluids during late stage volcanism is a major source of economic ore deposits. The deposits are called epithermal. Epithermal deposits are sources of Pb, Zn, Au, Ag, Hg, Sb, Cu, Se, Bi, and U, many of which occur as sulfides. The surrounding host rock is mineralogically changed during the injection of the ore bearing fluids. The mineralogical changes, termed hydrothermal alteration, produce a series of mineralogical assemblage zones which surround the ore deposit (Lowell and Guilbert, 1970).

Figure 4 is an idealized schematic from McMillan and Panteleyev (1980) and Gustafson and Hunt (1970). It presents the four major stages of alteration/mineralization. The post magmatic stage represents the intrusion of magma

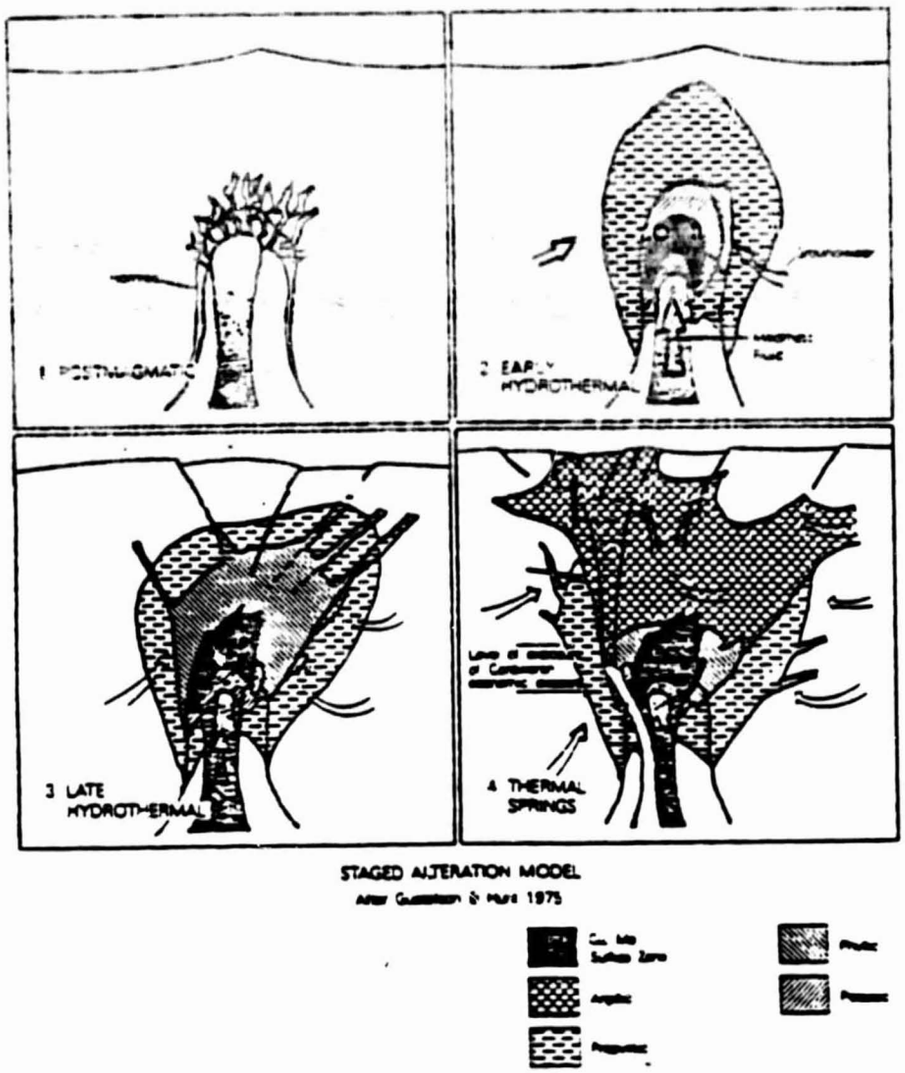

STAGED ALTERATION MODEL

Figure 4. Staged Alteration model. Idealized model showing sequential stages of alteration/mineralization. From McMillan and Panteleyev (1980) after Gustafson and Hunt (1975).

and the resulting thermal metamorphism. The upward flow of fluids and the increased cooling of the pluton results in increased fracturing and mass transfer (McMillan and Panteleyev, 1980). This comprises stage 2. The first two stages are the orthomagmatic contribution to alteration and mineralization. In these stages, the major portion of the fluid is derived from the magma. The resulting alteration reactions are prograde. The hydrothermal processes occur at high temperatures (600 - 700 °C).

Later alteration/mineralization is represented by stages 3 and 4. These stages comprise the convective contribution in which circulating meteoric water is the principal fluid source. Groundwater circulates through the fracture system producing a cooler, more acidic environment. At temperatures below 300 °C, reactions such as the following occur in which acid hydrolysis of feldspar and muscovite produces kaolinite:

$$\underset{\text{K-spar}}{3KAlSi_3O_8} + 2H^+ \leftrightarrow \underset{\text{muscovite}}{KAl_3Si_3O_{10}(OH)_2} + \underset{\text{Quartz}}{6SiO_2} + 2K^+$$

$$\underset{\text{muscovite}}{2KAl_3Si_3O_{10}(OH)_2} + 2H^+ + 3H_2O \leftrightarrow \underset{\text{kaolinite}}{3Al_2Si_2O_5(OH)_4} + 2K^+$$

(Rose and Burt, 1979)

Argillized zones are produced as the system cools and becomes weakly acidic. This final stage is represented by stage 4.

The surface exposure of an altered/mineralized rock unit is often a series of alteration zones. The most in-

Table 1. Idealized mineral assemblages associated with alteration zones. Compiled from Hunt and Ashley (1979) and Lowell and Guilbert (1970).

Zone	Mineralogy
Propylitic	Albitized Plagioclase
	* Chlorite
	* Epidote
	* Carbonate
	* Montmorillonite
Argillic	Quartz
	* Kaolinite
	* Chlorite
	* Montmorillonite
Phyllic	Quartz
	* Sericite
	Pyrite
Advanced Argillic	Quartz
	* Alunite
	* Pyrophyllite
	* Kaolinite/Dickite
	Opal
	* K-Mica
Silicified	Quartz
	* Alunite
	* Pyrophyllite
	* Kaolinite/Dickite
	* K-Mica

* = minerals with VNIR spectral features.

tensely altered rock occurs closest to the intrusive. This intense alteration is contained in the silicic and potassic zones. The degree of alteration decreases away from the intrusion through the phyllic and propyllitic zones until unaltered host rock is reached. Table 1 is an idealized list of the mineral constituents of each zone. Often associated with each zone is an intense iron staining produced by the oxidation of pyrite. Pyrite oxidation produces hematite, goethite, and jarosite. The resulting assemblage of alteration zones and iron staining is called a gossan.

The ferric minerals, goethite, hematite, and jarosite, contain Fe^{+3} in octahedral coordination. Fe^{+3} is a d^5 metal and undergoes spin dis-allowed crystal field transitions in all three minerals. The transitions are superimposed on a more intense O^{2-}--Fe^{+3} charge transfer centered in the ultraviolet portion of the spectrum. Each mineral has a unique spectrum due to differences in the geometry of the sites occupied by iron. Figure 5 shows the spectra of these minerals which occur within the VNIR portion of the spectrum.

Clay minerals and sulfates are shown in table 1 to be major alteration minerals which are often exposed on the surface overlying ore zones. Hunt and Ashley (1979) examined the reflectance spectra and mineralogy of altered rocks from the Goldfield mining district. Altered rocks produced spectra which contained an intense absorption feature near 2200 nm. They identified this feature as being

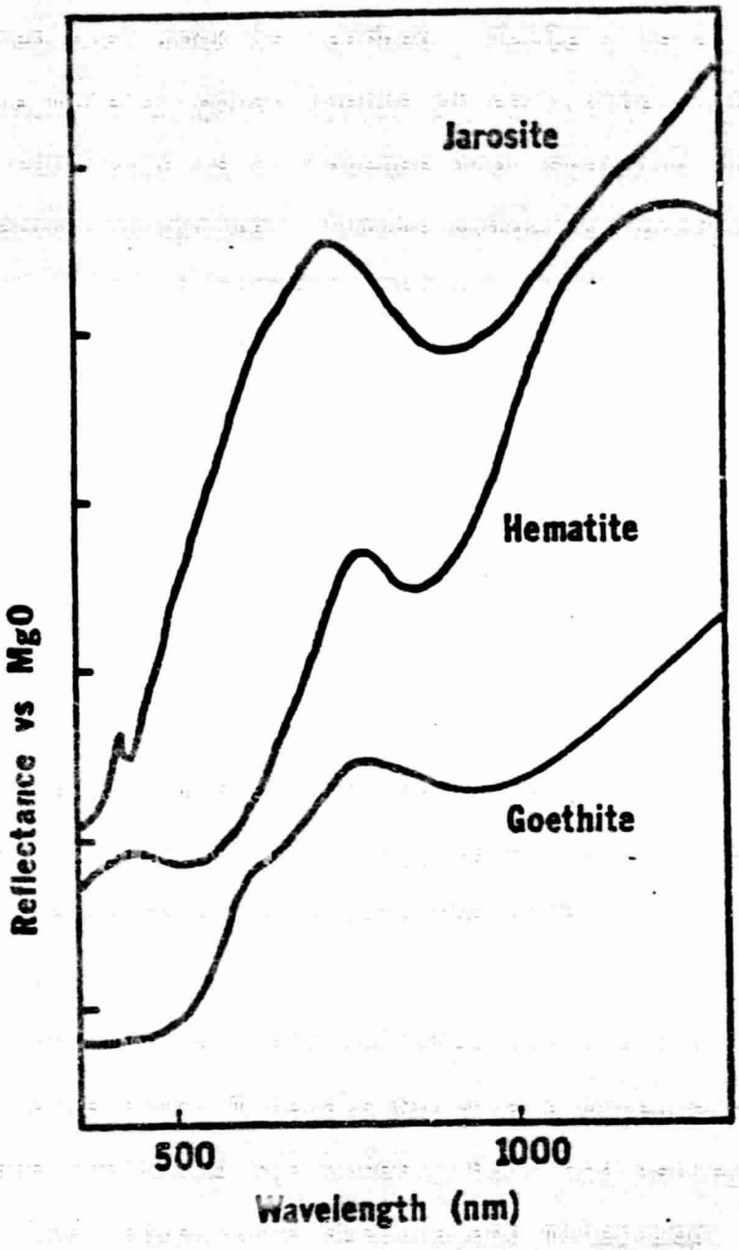

Figure 5. Visible-near infrared spectra of common Fe^{+3} bearing minerals associated with alteration zones. From Hunt and Ashley (1979).

due to a vibrational overtone produced by the principle hydroxyl stretch and the Al-OH bending mode. The position and shape of this feature was found to vary with mineralogy. Figures 6 and 7 shows the spectra of several minerals found by Hunt and Ashley in the altered samples from Goldfield.

Early Applications

ERTS-1, the first of the Landsat satellites, was launched in the early 1970's and produced images of the Earth in four spectral bands, 500 - 600 nm (band 4), 600 - 700 nm (band 5), 700 - 800 nm (band 6), and 800 - 1100 nm (band 7). The ground resolution of ERTS-1 was 79 meters square. The spectra of the three major ferric iron gossan constituents contain absorption features near 900 nm and 400 nm (Figure 5). All three minerals would produce low reflectance values in band 4 and in band 7.

The Goldfield, Nevada, mining district is the site of epithermal ore bodies (Ashley and Keith, 1978) with associated hydrothermal alteration. Rowan, et al. (1974) attempted to delineate the alteration at Goldfield through the use of Landsat imagery. They ratioed the intensities of the Landsat bands to construct the composite bands 4/5, 5/6, 6/7. They created a composite image by assigning a color to each band ratio and printing an image of all three colors. Within this image, called a false color ratio composite, altered areas with high iron content were discernable by their unique green color. Altered rock with low iron con-

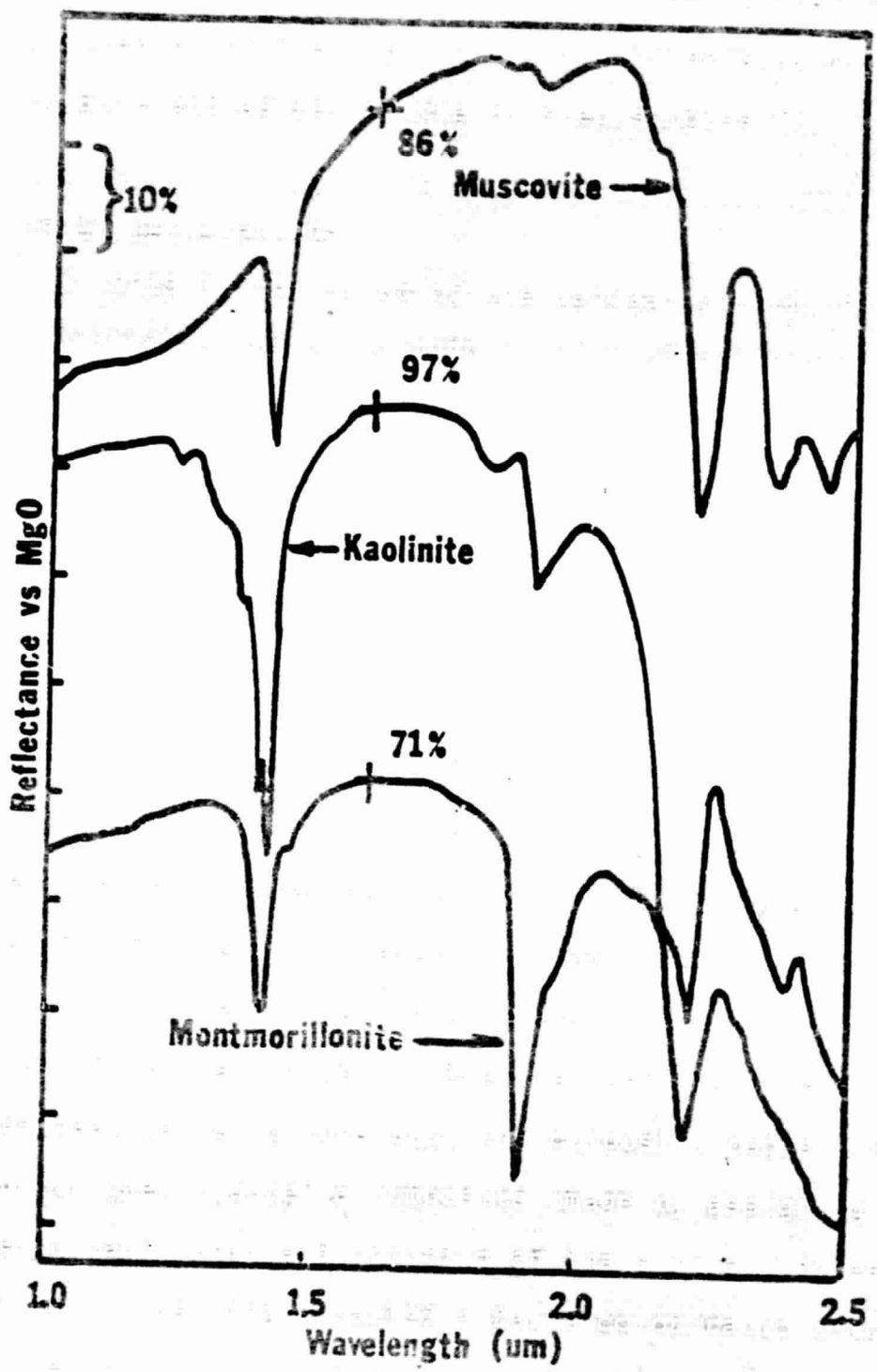

Figure 6. Near infrared spectra of several clay minerals associated with alteration zones. Adapted from Hunt and Ashley (1979).

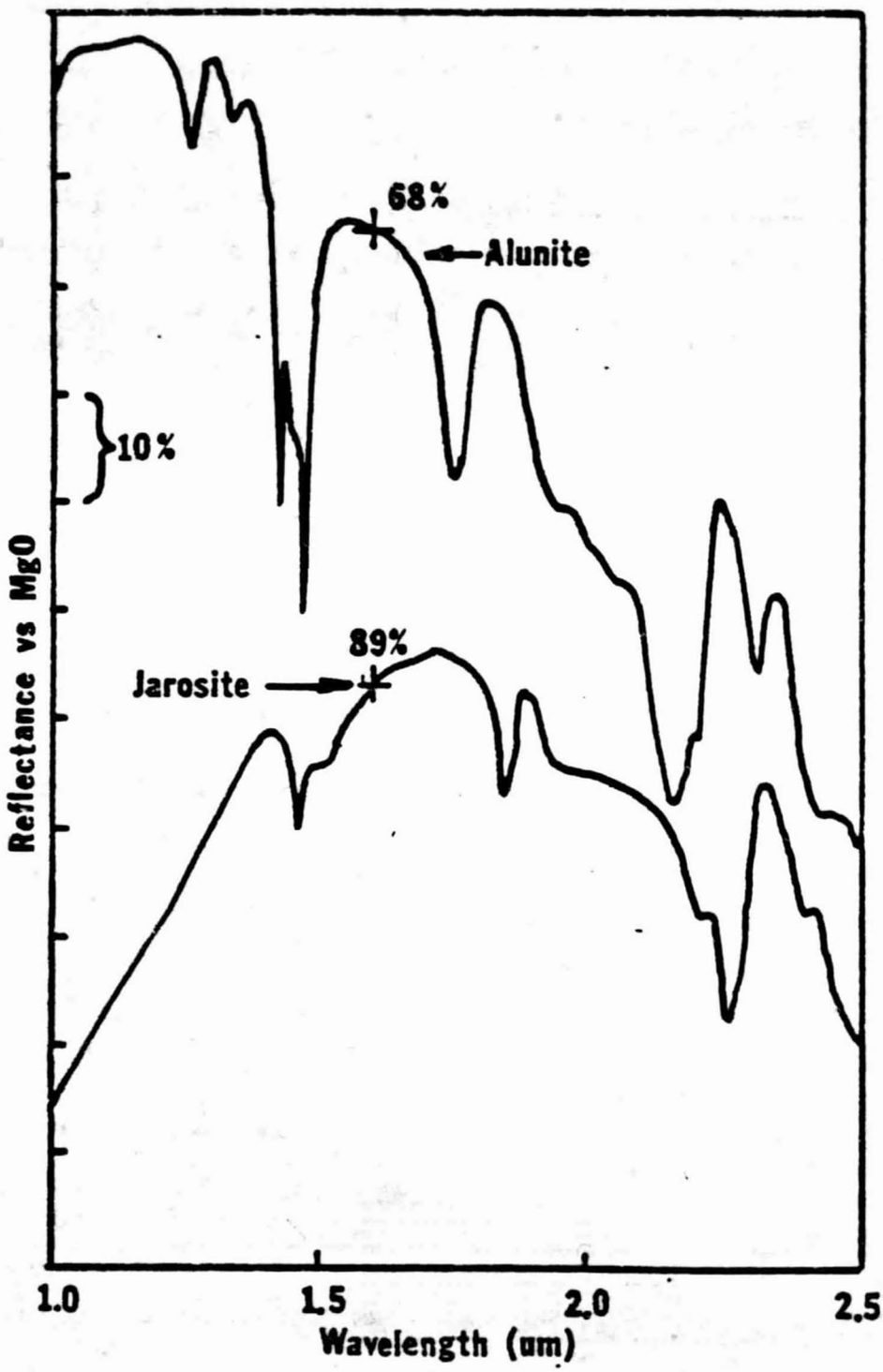

Figure 7. Near infrared spectra of jarosite and alunite. From Hunt and Ashley (1979).

tent was undetectable. Unaltered rock with high iron content had the same green color as the altered rock. It was concluded that the ferric signal alone was not diagnostic for delineating hydrothermally altered areas.

The hydrothermal alteration of the Cuprite, Nevada, district was studied by several researchers (Abrams, et al. 1977; Rowan, et al. 1977; Ashley and Abrams, 1980). Abrams, et al. (1977) utilized an aircraft mounted multi-spectral scanner equipped to measure reflectance intensities in hydroxyl and Al-OH vibrational overtone region (2200nm) as well as in the ferric absorption band. Using the ratios 1600/2200 nm, 1600/480 nm, and 600/1000 nm, hydrothermal alteration could be delineated with or without a ferric oxide coating. If unaltered rock in the area also contained hydroxyl bearing minerals, they would also be classified as altered.

In another study, Rowan, et al. (1977) used a portable field spectrometer in the Goldfield mining district. The field spectrometer was equipped to record reflectance spectra between 0.4 μm and 2.4 μm, thereby including ferric absorption and hydroxyl absorption. They found altered rocks to have an overall higher reflectance due to high clay and alunite content. Altered rock spectra contains a reflectance minimum centered near 2.2 μm due to clay minerals and alunite. Using a ratio of reflectance intensities recorded at 1.6 μm and 2.2 μm, clay content could be examined and altered areas could be defined with or without a ferric

coating. The 1.6 μm band was used because it is a reflectance maximum on most spectra. The major problem in this method was the inability to discriminate between altered rocks and iron stained rocks, such as unaltered hematitic metasediments. The metasediments have a strong clay absorption due to the clay minerals originally contained in the rock before metamorphism. Subsequent studies have used different statistical and computational treatments of Landsat and aircraft data (Podwysocki, 1979; A. Watson, 1979; Kahle, et al., 1979), the inclusion of structural features associated with alteration (Raines, 1978; Gornitz, 1979), and the use of thermal IR data (Kahle, et al., 1979, 1980; Kahle and Rowan, 1980; Watson, 1979; Pratt, et al., 1978).

A major difficulty in mapping hydrothermal alteration using reflectance imagery, has been in discriminating the clay and iron oxides present in an altered rock from those found in unaltered rock. Any differences that exist must have either the addition of hydrothermal fluids or a differing weathering regime as its source.

Aluminum Substitution in Iron Oxides

Iron oxides are common weathering products in many weathering environments. Recently, the identification and characterization of fine grained iron oxides in soils has shown that hematite and goethite are not the same in all environments. Several laboratory studies have shown aluminum to easily substitute for iron in these minerals (Thiel,

1963; Norrish and Taylor, 1961; Schwertmann, 1977, 1979; Golden, 1978; Golden, et al., 1979). Bigham (1977), Golden (1979) and Kodama (1977) have shown that both hematite and goethite have variable degrees of aluminum substitution in their crystal lattices. Fitzpatrick (1979) reports that the aluminum content depends on pH and a source for the aluminum. At both very high and very low pH's, no aluminum was incorporated in iron oxides, presumably due to the high solubility of aluminum under those conditions. Bigham, et al. (1978) have shown that high aluminum content is quite common in oxisols and ultisols in the United States. Nahon et al. (1977) have shown the ability of aluminum substituted goethite to react to form aluminum substituted hematite in soil horizons in Senegal. Golden (1979) has shown the incorporation of aluminum in goethite causes a decrease in particle size and a change in grain shape, as well as affecting a variety of soil properties.

It is likely that a difference exists in aluminum content of iron oxides overlying ore bodies from iron oxides with unaltered minerals as their source. Ore minerals are emplaced as sulfides into the surrounding host rock. The iron stained leached zone, which is the indicator of underlying mineralization, is produced through the weathering of the sulfide minerals. The iron oxides presumably form from the oxidation of pyrite and other sulfides (Blanchard, 1968). The clay minerals form from either the initial attack of hydrothermal fluids on the host minerals or from

the low pH fluids produced during the weathering of sulfide constituents. Blanchard (1968) reports pH values between 1 and 2 commonly occur in the production of sulfuric acid associated with sulfide weathering. Aluminum is commonly a residual element in most weathering environments, being nearly insoluble between pH values of 4 and 9 (Mason, 1966). Below pH 4 and above pH 9, however, aluminum is soluble. Fitzpatrick (1979) found iron oxides produced under extreme pH conditions, either high or low, to be relatively free of aluminum. It would therefore be likely that iron oxides in gossans to be relatively aluminum free, while those formed under common weathering conditions to be higher in aluminum content.

The degree of aluminum substitution in gossan iron oxides may be an indicator of alteration but it will only be useful in remote sensing if it leads to a recognizable signal in the material's remotely sensed spectrum. The 900 nm absorption features commonly associated with hematite, goethite and jarosite are crystal field transitions. Specifically, they are the $6A_1 \rightarrow 4T_1g$ transition for each mineral. The partial substitution of aluminum for iron may affect this transition. Fe^{+3} in an octahedral field, which is the case for these three minerals, has the degeneracy of its d shell orbitals split into two levels, eg and t_2g. The difference between these levels is the crystal field splitting parameter 10 Dq. Dq is an inverse function of the interatomic radius, r. Since Al^{+3} is smaller than Fe^{+3}, a dis-

tortion of the crystal structure occurs when Al^{+3} is substituted. The distortion results in a decrease in crystal d spacing and should also lead to a change in the interatomic radius. This change in r should lead to a change in Dq which would cause a shift in the crystal field transitions. (See Appendix A).

Other minerals besides iron oxides are also gossan constituents. It is likely that these too would differ from minerals in unaltered rock. In arid environments, clay minerals would form at a much lower rate than in a temperate environment. The lack of rainfall would lead to a lower rate of chemical weathering. Clays are formed readily in zones of hydrothermal alteration. They are produced either by the initial attack on host rock minerals by hydrothermal solutions or by the subsequent attack by sulfuric acid produced in sulfide weathering. Therefore, the concentration of clay minerals and the intensity of their 2.2 μm absorption feature may be another indicator of alteration.

Iron and aluminum sulfate minerals occur in some but not all hydrothermally altered areas (Blanchard, 1968; Meyer and Hemley, 1967; Hurlbut, 1971). These minerals, namely jarosite and alunite, are positive indicators of alteration but their absence does not indicate non-alteration, due to their restricted emplacement. They are useful in remote sensing since they have characteristic spectral features which occur in atmospheric windows.

It can be seen that there are a number of minerals which may be useful in delineating ore bodies by remote sensing. There is a gap in present remote sensing research. Several studies have been conducted on the reflectance properties of mineralogically characterized particulate samples under laboratory conditions (Hunt and Salisbury, 1970 - 1974 series). As mentioned earlier, there have been several studies on the remotely sensed spectral properties of mineralized areas. There have been several studies (Hunt and Ashley, 1979; Conel, et al., 1978) in which hand sample mineralogy was combined with field spectra from aircraft. This led to the general conclusion that clay minerals were the source of the 2.2 mm absorption feature and the 0.9 mm feature was due to ferric iron. A problem in these studies was relating laboratory spectra to field spectra to mineralogical analysis. Hunt and Ashley (1979) examined rock samples, homogenized and ground <74 μm, both mineralogically and by reflectance. Since field samples consist of a rock unit with an overlying weathering rind, grinding and homogenizing a rock sample has the effect of diluting the surface material with underlying fresh rock. The depth of penetration of visible-near IR radiation has been reported to be ≈4 λ's for solid crystals (Kortum, 1968) to several millimeters for ground, unabsorbing material. Therefore, a remote sensing signal will mainly reflect the surface mineralogy while the laboratory procedure used by Hunt and Ashley will reflect the bulk composition. The two

portions of the sample, surface and bulk, need not be similar. Some rock coatings, such as desert varnish, are proposed to be derived from wind blown clays and oxides, and are compositionally different from the underlying rock (Potter and Rossman, 1978). The mineralogical characterization of altered and unaltered rock for remote sensing becomes an analytical problem in characterizing only the surface weathering products which contribute to a remotely sensed signal. The inital step must be a measurement of the depth of penetratiion of visible-near IR radiation into the weathering rinds. This depth will define that portion of the rock which interacts with the incident radiation, and will be referred to as the "optical depth" throughout this study.

Analysis of Rock Surfaces

In order to characterize the minerals which produce a rock's reflectance spectrum, the analytical procedures must be devised to analyze only the upper rock surface down to the optical depth. Several researchers have worked on a similar problem, the characterization of desert varnish (Potter and Possman, 1977; Allen,. 1978; Hooke, et al. 1969). Desert varnish is a dark, manganese rich coating which forms on desert rock surfaces. It has a limited thickness and therefore the analytical problem encountered was similar to the analytical problems in this study, namely, how to mineralogically characterize a thin coating

in which mixed clay and x-ray amorphous ferric minerals occur.

Ferric oxides and oxyhydroxides have been reported as the major, non-clay constituents of rock surface coatings in arid environments (Potter and Rossman, 1977; Hooke, et al., 1969). A variety of manganese oxides and oxyhydroxides have also been reported. The mineralogic analysis of ferric constituents presents special problems due to their occurrence as coatings, their low concentrations, and their existence often as mixed phases.

Allen (1978), in a characterization study of desert varnish, avoided the mineralogic problem by mapping total iron concentration on cross sections of rock coatings. In this manner, he was able to measure the thickness of the coating to be approximately 20 μm but could not say what oxide phases were present. Engle and Sharp (1958) ground the coatings from their samples and spectroscopically measured iron concentration as varying from 1 to 5 weight percent iron. However, their percentages were calculated after assuming a 50% correction factor due to inclusion of underlying ground rock. Hooke, et al. (1969) studied desert varnish coatings intact with the microprobe and found the coatings exhibited a leached zone between the fresh rock and the iron rich coating. He found a relationship, between the topography of the rock surface and the coating thickness; explaining this as being due to the transportation and deposition of iron and manganese from water. Potter and Rossman

(1977) chemically extracted iron rich desert varnish coatings and also examined the coatings in situ using an electron microprobe. They found the iron and manganese content varied from 10% on the underside of the rock to 30% on the upper surfaces. They concluded the oxides occurred as discrete coatings on clay minerals due to their effect on clay expandibility. Due to a lack of a leached zone on the analyzed samples, they concluded the coatings are externally derived from a wind blown source. In a later study (Potter and Rossman, 1978), an epitaxic relationship between wind blown clay and water borne iron and manganese oxides was proposed. According to this hypothesis, wind blown clay adheres to rock surfaces and acts as a template for manganese and iron oxides to form. In this study, near IR spectroscopy was used to identify the iron phase as hematite.

Therefore, it appears that a mineralogical characterization of a thin, discrete surface can be accomplished. The microprobe can be used to observe zoning and leached zones which may yield information on the genesis of the surface coating. Due to the width of the absorption features used to identify ferric oxides, IR spectroscopy is not an ideal technique for identifying surface minerals unless it is used in conjunction with other methods.

The study of fine grained, discrdered iron oxides in soils was undertaken by several researchers. Bigham, et al. (1978) and Kodama, et al. (1977) initially attempted to identify soil iron oxides by x-ray diffraction. The iron

oxide constituents in soils often occur as coatings on clay particles. X-ray diffraction in this case was not useful in determining iron mineralogy. Due to the fine particle size, low concentrations, and lack of long range order, the diffraction peaks were broad or not resolved. Several of the major peaks overlap with more plentiful soil minerals, such as quartz.

A concentrating technique reported by Norrish and Taylor (1961) in which samples are boiled in 5N NaOH proved effective in dissolving aluminosilicates and leaving iron oxides as residuals. This process, however, has been reported as possibly converting aluminous goethites to hematite (Petit, et al., 1964). This technique was subsequently studied by Bowen and Weed (1980) and found to not leach aluminum from iron oxides as long as other aluminum rich minerals were present.

The iron oxides of interest in this study also occur as discrete phases in soils. Mossbauer spectroscopy has been utilized by a number of researchers to identify iron minerals in soils (Kodama, et al., 1977; Bigham, et al. 1978; Golden, et al., 1976; Schwertmann, 1977).

In the previously cited studies by Bigham, et al., (1978) and Golden, et al. (1976), the effective field was found to be useful in determining which oxide phase was present. Golden's study produced an inverse linear relationship between mole percent substituted aluminum and the intensity of the effective field. Bowen and Weed (1980)

showed a similar trend for the effective field measured at room temperature and the percent substituted aluminum in hematite.

It appears that a combination of Mossbauer spectroscopy, electron microprobe analysis, x-ray diffraction, and selected chemical techniques will provide the mineralogical ground truth necessary to relate reflectance spectroscopy to mineralogy.

ANALYTICAL METHODS

Introduction

Answering the questions posed in this study required the use of several analytical methods and the interpretation of a variety of data sets. This chapter will discuss the experimental design of this study. It will describe the rationale for using each analytical method.

Attempting a characterization of the portions of natural rock samples that contribute to remotely sensed reflectance spectra requires a measurement of the depth of penetration of energy into the rock within the wavelength region of interest. To measure this depth of penetration, which is defined here as the sample's optical depth, synthetic samples which texturally and compositionally modeled natural rock weathering surfaces were utilized. The use of synthetic rather than natural samples allowed a greater degree of control over homogeneity and compostiion.

The next section concerns the characterization of aluminum substituted iron oxides. This was necessary since it was felt that the incorporation of aluminum into the iron oxides might be an indication of unaltered rock. The experiments were designed to examine the effect of aluminum substitution on the crystal field transition spectra of hematite and goethite. Natural and synthetic samples were first characterized by several techniques and then analyzed by reflectance spectroscopy.

The third section contains the mineralogical analytical techniques utilized in the examination of natural rock and soil samples from several mining districts in western Nevada. A variety of analytical techniques were utilized to identify the minerals present and to relate them to the laboratory spectra. Many of the techniques used in the analysis of field samples were also used in characterizing the synthetic samples.

Optical Depth Determination

The ultimate question to be answered in this study was to note if any mineralogic differences exist between hydrothermally altered rocks and unaltered, weathered rocks. To be useful in remote sensing, any difference which may exist must produce an absorption feature in a portion of the electromagnetic spectrum which is observable through the atmosphere.

The initial problem, therefore, was to measure what portion of a rock or soil surface contributed to the rock or soil's reflectance spectrum. That portion might then be analyzed by any analytical technique which would identify mineral phases, and the phase identifications could be correlated with the rock or soil's reflectance spectrum.

Judd, et al. (1937) studied the diffuse reflectance properties of a number of solid samples including paints, silicate cements, and paper. They found a linear relation

ship between reflectance intensity, as represented by the log of the Kubelka-Munk function, and sample thickness.

In order to use the Kubelka-Munk function to represent reflectance, certain criteria must be met. Primarily, the sample must be a diffuse reflector (Kortum, 1968). This is achieved through the use of a reflecting sphere. Secondly, the sample's width must be much greater than its thickness in order to avoid any edge effects. If these conditions are met, the reflectance value at any wavelength can be treated as a diffuse reflectance value.

Ensuring diffuse reflectance is important for this experiment. Janza (1975) notes that a sensor viewing the Earth from a vertical position, with the solar irradiance striking the surface at a high angle, causes the surface to behave as a diffusely reflecting, or matte, surface.

A review of the available literature showed the depth of penetration was wavelength dependant and was reported to vary from four times the wavelength (Kortum, 1968) in crystalline solids to several millimeters in ground powder samples (Judd, et al., 1937; Hunt, 1980). Since natural rock surfaces appear to be oxide and clay coatings formed from solution and the adhesion of wind blown particles (Potter and Rossman, 1977), neither a solid crystalline or a ground powder model seemed to fit the structure of natural samples. A series of synthetic samples with controlled composition and particle size and whose thickness could be easily measured were employed. In this experiment, a number of

sample "suites" were made. Within a single suite of ten samples, composition and particle size were constant. The thickness of each succeeding sample was increased so that a single suite covered a range of thicknesses from approximately 5 to 60 μm. Each suite contained a mixture of iron oxide and a clay mineral. The iron oxide was either hematite, goethite, or aluminmum substituted goethite. The clay mineral was either kaolinite, montmorillonite, halloysite, or pyrophyllite. These minerals were utilized since they are common components of the weathered zones overlying ore deposits (Blanchard, 1968; Hunt and Ashley, 1979). The weight percent of each phase in each suite is listed in Table 2.

Each suite was produced by grinding the pure components under acetone and centrifuging the ground powder the time and speed required by Stokes' settling law to obtain the required particle size. The resulting sized sample was dried and weighed. It was mechanically mixed with the weighed portion of the second mineral of the suite and then suspended in water in a 500 ml volumetric flask. Aliquots of the suspension were filtered through Millipore 0.45 μm filters and allowed to dry. To make thin samples, a small aliquot was used. The flask was shaken before taking each aliquot to ensure homogeneity within each suite.

The visible-near IR (450 nm - 2500 nm) reflectance spectrum of each sample was collected on a Cary 14 spectrophotometer fitted with a MgO coated reflecting sphere. A

Table 2. Composition of sample suites utilized in optical depth experiments.

Suite #	Weight % Oxide/ Weight % Clay	Oxide	Clay
1	25/75	goethite	kaolinite
2	50/50	goethite	kaolinite
3	75/25	goethite	kaolinite
4	100/0	goethite	
5	25/75	hematite	kaolinite
6	50/50	hematite	kaolinite
7	75/25	hematite	kaolinite
8	100/0	hematite	
9	50/50	Al-goethite	halloysite
10	25/75	Al-goethite	halloysite

100% reflectance scan was run using a $BaSO_4$ standard before and after each 10 samples. After collecting the reflectance spectrum, each sample was cut and mounted edgewise on an aluminum sample mount. Care was taken not to disturb the cut edge. The thickness of the clay-oxide mixtures was measured on an ISI scanning electron microscope.

Aluminum Substitution in Iron Oxides

Introduction

As noted previously, aluminum substitution for ferric iron is a common geochemical occurrence. Due to their similar charge/radius ratio, they substitute for each other in a number of mineral sites.

If the degree of aluminum substitution in iron oxides is related to the oxide's environment of formation, then the degree of substitution may be an indicator of hydrothermal alteration. In order for this to be useful in remote sensing, the substitution of aluminum must cause a change in the ferric iron visible-near infrared reflectance spectrum.

Sample Preparation

Synthetic aluminum substituted goethite samples were prepared by the methodology developed by Thiel (1963) and amended by Jonas and Solymar (1970) and Golden (1978). In general, the goethites were prepared by mixing a ferric/aluminum nitrate solution with NH_4OH. A yellow/brown

precipitate formed which was centrifuge washed and heated in a Parr bomb. On the first attempts at this synthesis, the reactants were mixed too quickly, and mixed phases resulted.

The first procedural change was the mixing of the precipitate with 2.0 N KOH after the centrifuge washing. The KOH contained some $Al(NO_3)_3 \cdot 9H_2O$, the amount depended on the aluminum content of the precipitate. Golden (1978) was used as a guide to the amount of $Al(NO_3)_3 \cdot 9H_2O$ to add to the KOH.

A second procedural change was attempted but later discarded. In order to produce a narrow compositional range, it was felt that the NH_4OH solution should be added dropwise to the mixed Fe/Al nitrate solution rather than the reverse. This did produce narrow, intense peaks on the x-ray diffraction pattern, but only hematite was produced.

Sample Analysis to Measure the Degree of Substitution

The initial part of this problem was to prove aluminum was not coexisting as a separate phase but was substituting into the goethite structure. This was accomplished through the used of x-ray diffraction and Mossbauer spectroscopy. A linear change in diffraction d spacing has been used to study a number of solid solution series. Mossbauer spectroscopy is useful since ^{57}Fe's effective field (H_{eff}) is affected by nearest neighbor cations (Greenwood and Gibb, 1971) and would not change if aluminum was occurring as discrete crystals of diaspore, the 100% aluminum end member.

X-Ray Diffraction

X-ray diffraction was used to measure the amount of aluminum substitution in the goethite structure. The synthetic samples, unlike most natural goethite samples, were sufficiently crystalline to be examined by x-ray diffraction. A decrease in d spacing has been shown to vary with aluminum substitution in the goethite structure (Thiel, 1963; Jonas and Solymar, 1970; Golden, 1978).

The synthetic samples were ground to pass a 325 mesh sieve (63 μm) and mounted with acetone in a drilled 7 mm depression in an aluminum sample block. The 2.34 A d spacing for aluminum metal was used as an internal standard and all peaks were measured from the center of the aluminum metal peak. The samples were irradiated with Cu K_a radiation at a scan rate of 1/2° 2θ/minute. A graphite monochrometer was used to screen out the iron fluorescence.

Mossbauer Spectroscopy

A technique which can be utilized to examine iron mineralogy is Mossbauer spectroscopy. The Mossbauer effect is the emission and absorption of gamma rays without nuclear recoil or thermal broadening. The fraction of emitters (f) which will emit, recoil free, will increase when the probability of exciting lattice vibrations is decreased. This probability of exciting lattice vibrations increases with increasing γ ray energy. This sets a maximum nuclear transition energy for which the Mossbauer effect will be

observed. ^{57}Fe is one of the isotopes in which the Mcssbauer phenomenon is observable. The first excited state decay of ^{57}Fe to its ground state is 14.4 KeV. The excited state is easily populated by ^{57}Co.

By accelerating the ^{57}Co source in relation to the absorbing ^{57}Fe sample, a spread of energies due to the Doppler effect is achieved. This spread is large enough to measure the differences in the absorber due to the particular chemical environment in which the absorbing Fe resides. The parameters which are measurable are the chemical isomer shift, the quadrupole splitting, and the effective field.

The chemical isomer shift is useful in determining the iron oxidation state. Since all of the iron minerals of interest in this study contain ferric iron, the isomer shift will be nearly equal for all samples.

The quadrupole splitting arises from the interaction of the quadrupole moments of the excited ^{57}Fe nucleus and the electric field gradient produced by the electronic orbitals and the distribution of lattice charges. It is therefore sensitive to and characteristic of the coordination geometry about the absorbing iron nuclei.

The third Mossbauer parameter is the effective field. The minerals in this study are either ferromagnetic or antiferromagnetic, therefore the ^{57}Fe nuclear energy levels may be split through interactions with the internal magnetic field. The magnitude of this splitting is proportional to the strength of the effective field.

As a second check on the composition of the aluminum substituted goethite samples, Mossbauer spectroscopy was utilized. Mossbauer and computer facilities at Catholic University of America, Washington, D.C., were utilized through the cooperation of Dr. Leopold May. The samples were run at liquid N_2 temperature using a ^{57}Co source and a scintillator detector. The data were collected in a 400 channel multichannel analyzer. A Lorentzian least squares fitting program, MOSE, was used to plot and measure the peak positions. Iron foil was used as a standard. For the iron foil standard, the H_{eff} value was known from the literature to be 330 $\pm$ 10 kG. The splitting between peaks 1 and 6 (Δ_{1-6}) in mm/sec, is proportional to the H_{eff}. The following relationship was utilized to yield the H_{eff} value for the samples:

$$\frac{\text{Sample } H_{eff}}{\Delta_{1-6}} = \frac{\text{Foil } H_{eff}}{\Delta_{1-6}}$$

The effective field values were used to determine aluminum content in each sample. Previous studies had shown a linear relationship between the degree of aluminum substitution in goethite and the Mossbauer effective field measurement (Golden, 1978; Bigham et al., 1978).

Visible-Near Infrared Reflectance Spectroscopy

It was necesary to see if aluminum substitution in goethite caused a shift in goethite's reflectance spectrum

in order for substitution to be important for remote sensing. Four of the substituted samples were sent to the U.S. Geological Survey-Denver for analysis by Dr. Graham Hunt. The samples were run on a Beckmann 5270 spectrophotometer equipped with a reflectance attachment. The ground samples were mounted in an aluminum cup, tamped flat and analyzed from 400 to 2400 nm.

The reflectance spectrum of each sample was reexamined on a Cary 14 reflectance spectrophotometer. The samples were scanned from 400 to 2500 nm. The analog recording was converted to digital format using a digitizing board and cursor. The position of each reflectance minimum was located by converting each digitized spectrum to its first derivative.

A series of natural, iron rich soil samples were also used in this study. Eighteen soil samples from central Texas were obtained from Dr. J. B. Dixon of Texas A & M University. The soils had been size fractionated by Dr. Dixon's laboratory. The iron mineralogy had been determined by x-ray diffraction and it was shown that the samples contained both aluminum substituted hematite and aluminum substituted goethite. The degree of aluminum substitution had been determined by x-ray diffraction and dithionite-citrate-bicarbonate extraction. In the present study, the x-ray diffraction results were rechecked. The soils were then analyzed by Mossbauer spectroscopy and visible-near infrared reflectance spectroscopy.

Visible-Near Infrared Reflectance Spectroscopy

Visible - Near Infrared (VNIR) reflectance spectral data were collected through three different methods in this study. The three devices utilized were:

1. the Shuttle Multispectral Reflectance Radiometer (SMIRR)
2. Hand Held Ratioing Radiometer (HHRR)
3. Beckmann 5270 Reflectance Spectrophotometer

SMIRR

SMIRR is a non-imaging remote sensing device designed for service aboard the second space shuttle flight. It is equipped to receive reflected radiation in ten bands (Goetz and Rowan, 1981). Figure 8 is a schematic of the band pass filters utilized on SMIRR. SMIRR was mounted on a JPL aircraft and test flown over several of the field sites examined in the present study. 16 mm photographs were automatically taken at each 128th radiometer sample. The sites which were mineralogically sampled on the ground corresponded to the centers of the 16 mm photographs to ensure correlation between radiometer and ground sampling. Strip chart recordings were made of the absolute radiance values and the ratioed reflectance data collected from each flight line. Ratioed data was used in the present study rather than the absolute radiance values of each channel. It was found that the radiance values correlated with topographic features rather than composition (Goetz and Rowan, 1981).

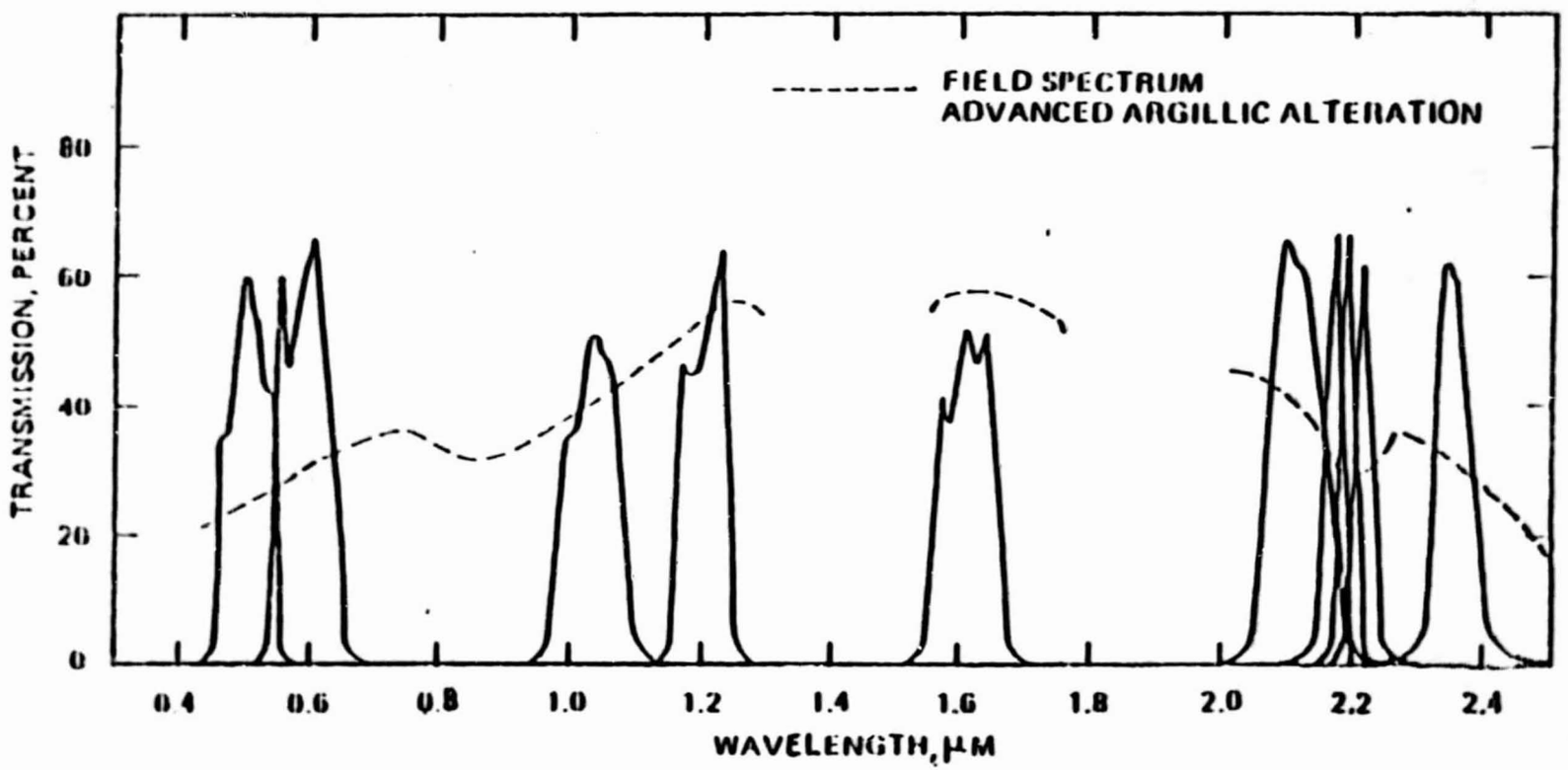

Figure 8. Band pass filters utlized by the shuttle multi-spectral infrared reflectance radiometer (SMIRR) from Goetz (1981).

The use of ratios eliminated the topographic effect. Table 3 is a listing of the ratios collected by SMIRR. A total of nine sites were hand sampled along the SMIRR flight lines. The nine sites provide compositional information for interpreting the SMIRR ratios.

HHRR

HHRR is a field portable, dual detector radiometer. A filter wheel was mounted in front of each detector. Each filter wheel contained six different band pass filters. Each detector simultaneously viewed the same 15 cm x 45 cm surface. The radiance values from the two detectors were ratioed and presented in a digital display. By placing different filters in each beam path, a variety of wavelength ratios were obtained. A set of five ratios were recorded at each sampling site. A total of 13 sites were sampled by HHRR. Three to six individual readings were recorded at each site for each ratio. The mean value for each ratio was reported. Before and after each site was sampled, the detector outputs were calibrated against a Fibrofax standard.

Laboratory Spectra

Each rock and soil sample was examined by VNIR reflectance spectroscopy in the laboratory. A Beckmann 5270 reflectance spectrophotometer was utilized. The instrument was equipped with a MgO coated relecting sphere and was run

Table 3. SMIRR Ratios. Spectral ratios collected during flights in western Nevada by the Shuttle Multispectral IR Reflectance Radiometer (SMIRR). Each ratio is comprised at two spectral bands. Each band is listed by its wavelength in μm.

Ratios
.5/.6
.6/1.05
1.05/1.20
1.20/1.60
1.60/2.10
2.10/2.17
2.17/2.20
2.20/2.22
2.22/2.35

from 2500 nm to 400 nm. The instrument's wavelength resolution was 2.5 nm. The soils were mounted in an attachment which allowed them to remain horizontal (Hunt, 1980a). The undisturbed rock surfaces were clamped against the sample port and analyzed. The instrument sampled a 5 mm x 10 mm rectangle of each sample surface. MgO was utilized as a standard. The output was recorded in analog form on a strip chart. Background and 100% reflectance values, using MgO as a sample, were recorded before and after the analysis of each group of 20 samples. The scan speed was 2 nm/sec in the 400 - 850 nm range and 4 nm/sec in the 800 - 2500 nm range.

Natural Sample Sites

Field sampling of natural rocks and soils was conducted over the three year period, 1978 - 1980. The sample sites were chosen to optimize the ability to discriminate hydrothermally altered rock from the surrounding unaltered rock. The criteria used to choose sampling sites were:

1. The existence of known hydrothermally altered rock at a sampling site and the close proximity of unaltered rock. This study was designed to note the ability of remote sensing to detect alteration, rather than locate previously undiscovered ore deposits.
2. The site should have limited vegetation and soil development. Vegetation has chlorophyll absorption

bands in the visible-near IR (figure 9) which may interfere with the bands associated with iron. Soils contain clay minerals. The production of clay minerals by hydrothermal processes is one of the signals available to a remote sensing device. Soils would appear to be altered rock to a sensor.

3. A clear and cloudless atmosphere was desirable. Clouds affect the signal received by portable field sensors and aircraft mounted sensors.
4. The availability of processed remote sensing data was necessary. This would provide a data set to compare to the compositional data.

Using the above criteria, a series of sites along the east side of the Sierra Nevada batholith were chosen (Figure 10). This portion of western Nevada is in the arid basin and range province. Vegetation is minimal, consisting of sagebrush, pinon pine, juniper, and other common desert flora. The sky is clear throughout much of the summer. There are a variety of hydrothermally altered areas throughout the region. Silver and gold vein deposits have been mined since the late 18th century. The alteration is often associated with early Tertiary rhyolitic to andesitic tuffs (Ross, 1961) and is located throughout Mineral, Esmerelda, and Nye counties. The following is a description of the sample sites:

Civet Cat (CC): Civet Cat canyon is a northeast-southwest trending canyon lying along, and perpendicular to, the

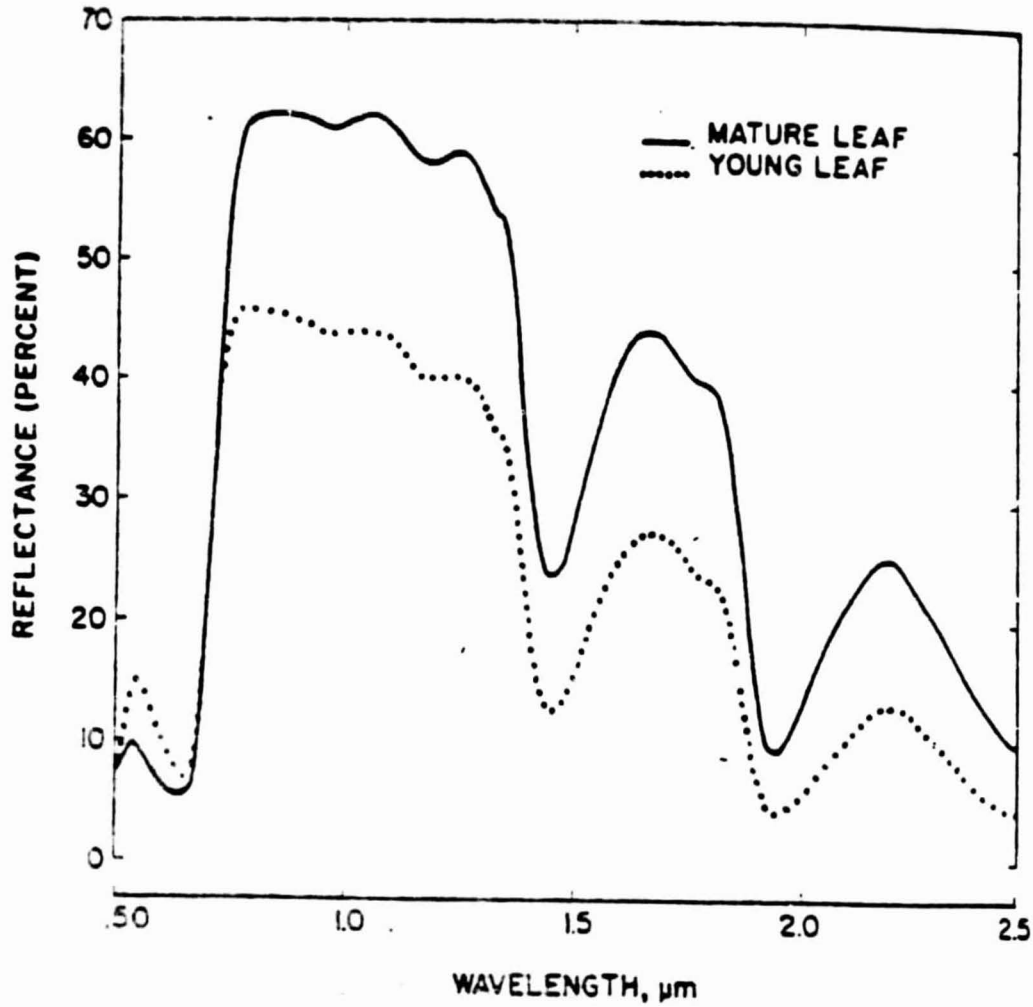

Figure 9. Visible-near infrared spectra of chlorophyl in several leaves. From Reeves (1975).

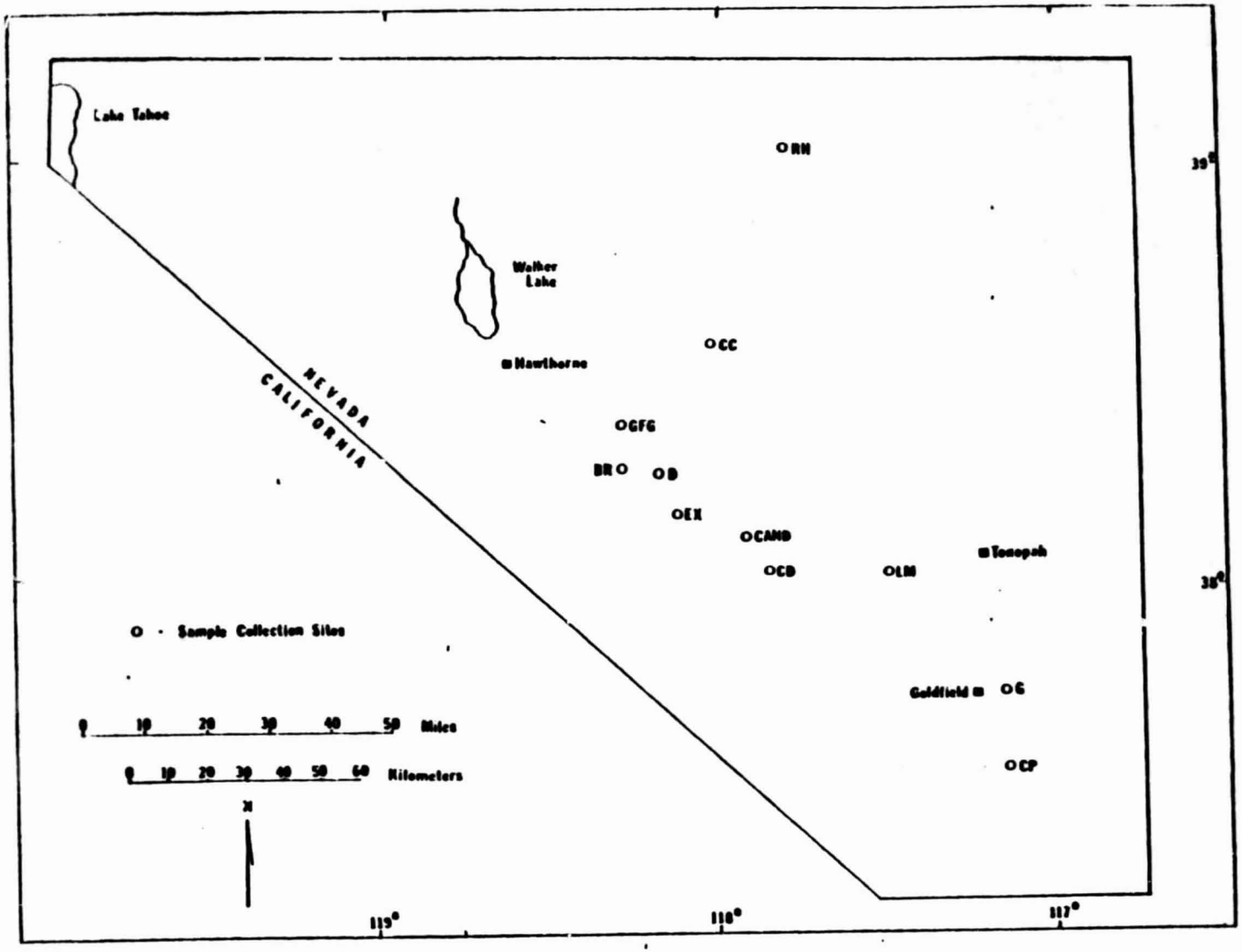

Figure 10. Map of sampling sites in south west Nevada. Letters near sites correspond to sample identifications.

Walker Lane fault 5 miles north of Luning, Nevada. The sampled rock unit is a silicified and argillized Tertiary ash flow tuff. It was coated by an orange-red iron staining at nearly all exposures. The alteration grades from silicified in the northeast terminus of the canyon, to propylytic at the southwest end. Samples were collected from both canyon walls along the complete length of the canyon.

Coaldale (CD): The Coaldale samples were collected from a low ridge on the south side of Route 6, five miles west of its intersection wioth Route 95 at Coaldale. The rock unit is an unaltered, iron stained, ash flow tuff.

Red Hills (RH): The RH samples were collected from the Monte Cristo Mountains, 10 miles northwest of Gabbs, Nevada. The rocks are iron stained tuffaceous sediments and silicic ash flow tuffs. All are Tertiary and unaltered.

Garfield Flats
Granodiorite (GFG): This is a Cretaceous granodiorite which outcrops northeast of Garfield Flats. It appears to be two distinct units. Unit 1 is a brown coated, exfoliated granodiorite which occupies topographic lows. Unit 2 is gray-black coated, and is not as weathered. It occupies the topographic highs. Both units were sampled as well as a number of aplitic dikes transecting the units.

Dunlap (D): Samples are from Garfield Flat, 10 miles southwest of Luning, Nevada. This unit is the Jurassic Dunlap formation. It is an iron-stained, feldspathic sandstone. It has the appearance of a desert pavement, occurring as a unit of rock shards rather than outcrops.

Barite Ridge (BR): Unaltered silicic tuff outcropping as a series of low hills west of Garfield Flat. Unit is iron stained and transected by quartz veins.

Excelsior (EX): Argillized and silicified silicic tuff northeast of Teels Marsh in the Excelsior Mountains. This unit was sampled along a dry wash heading west from Kerrick Mine.

Candelaria (CAND): An unaltered, iron stained, calcite cemented sandstone which occurs 15 miles northeast of Coaldale, Nevada. This area is a series of rather homogeneous, talus covered low hills.

Goldfield (G): The Goldfield mining district is the site of epithermal, bonanza ore bodies mined in the late 19th and early 20th century. The ore is associated with silicified zones in altered Miocene intermediate volcanics (Ashley and Kieth, 1978). Samples were collected along a SMIRR flight line from altered and unaltered andesites and dacites. The 1980 samples were collected from altered and unaltered portions of the same rock unit, Milltown dacite.

Cuprite (CP): The Cuprite mining district is 9 miles south of Goldfield and includes two exposures of hydrothermally altered rocks (Abrams, et al., 1977). The eastern exposure was sampled for the present study. Silicified, argillized, and opalized units of the altered Thirsty Canyon tuff were present in the exposure. Multiple samples were collected from the three altered zones as well as the nearby unaltered tuff. Several samples were collected from the southern portion of the silicified zone where it is coated by desert varnish.

Remote sensing data was available from three different instrument systems: Landsat, Shuttle Multispectral Infrared Radiomenter (SMIRR), and an instrument designed by Collins and Chang of Columbia University. The three different devices were flown at different times and have different characteristics. Landsat has 79 m ground resolution, is satellite borne, and is equipped with four visible-near IR bands. Collins and Chang's instrument is a non-imaging array of 500 detectors equipped to collect radiation from single points along a flight line. The ground resolution was approximately 4 m and the spectral region covered was from 450 nm to 1100 nm. SMIRR is a non-imaging system containing 10 channels of varying resolution (figure 8). Flown at an altitude of 2000 m, it had a ground resolution of 1 m.

Landsat Sampling

An image of the Walker Lake 2° sheet was constructed in which areas with a high ferric iron content were depicted (Rowan and Purdy, 1981). The image was utilized for locating sampling sites in the present study. High ferric content had been associated with alteration in Goldfield (Rowan, et al., 1974) and was being examined at Walker Lake (Rowan and Purdy, 1981). Areas, both altered and unaltered, with high ferric iron content were sampled throughout the Walker Lake quadrangle. Sites were located by correlating aerial photographs, 15 minute topographic maps, and the ferric iron Landsat image. Due to the low Landsat resolution, locations were approximate, and assumed to be within $\pm$ one pixel (79 m) of the true high iron site located on the Landsat image.

GISS Radiometer Flight Lines

The Collins and Chang multispectral radiometer was mounted in an aircraft and flown over several of the altered and unaltered rock units which were shown to have high ferric iron content on the Landsat Walker Lake image. A 35 mm photograph was automatically taken at each tenth radiometer sample. The photographs were utilized to locate the sample sites. Each tenth site was located in the center of a photograph. The intervening radiometer sites were interpolated between the centers of the photographs. Sampling was conducted along each flight-line and included the Civet Cat

(CC), Dunlap (D), Excelsior (EX), Coaldale (CD), and Monte Cristo (MC) flight lines.

SMIRR

SMIRR was flown over several flight lines which included the Lone Mountain (LM), Goldfield (G), Cuprite (CP), Candelaria (Cand), and Coaldale (CD) samples. The instrument took a photograph every 128th radiometer reading. The photographs were joined together to form a continuous strip. Through the use of an onboard clock, the time of the photographs could be correlated to the radiometer data. This allowed for the possiblility of well registered radiometer and ground samples. The centers of the photographs were used as sample sites since the registration between the ground and the radiometer was considered to be more exact. Between centers, the exact location sampled by the instrument was affected by aircraft pitch and roll. The sample sites were chosen where the flight lines crossed homogeneous rock units.

At these sites, field radiometer data was collected with a Hand Held Ratioing Radiometer (HHRR). Rock samples were gathered from the same areas covered by HHRR. Soil samples were collected from the top 3 - 5 cm of each site's soil. Photographs were taken at each site. The samples were sealed in marked plastic bags.

Due to the better correlation to remote sensing data provided by the SMIRR samples, their analysis was used to

provide compositional ground truth for remote sensing. The Landsat and Collins and Chang samples were used to provide mineralogical differences between altered and unaltered rock. Due to the lower ground resolution, exact ground locations corresponding to radiometer sampling sites could not be ascertained. These samples were not used for ground truth due to this lower degree of confidence in the actual sites to be sampled.

Thin Sections

Thin sections were prepared from 15 rock samples. The samples represented altered and unaltered rocks from several mining districts in western Nevada. Their upper surfaces were analyzed by visible-near IR reflectance before being sectioned. The thin sections were all cut cross-sectionally to a size that would fit in the electron microprobe. This was done in order that cross-sectional mapping and elemental analysis of the surface coating could be performed on the microprobe.

Microprobe analysis was performed on selected thin sections. Iron, aluminum, and sulfur elemental maps were constructed. The sections were also analyzed using an ISI scanning electron microscope. The samples were carbon coated and the thickness of the upper weathering surface was measured.

Digitized Spectra

The analog output of all visible-near IR reflectance analysis was converted to digital format through the use of a digitizing board and cursor. Analog to digital conversion was necessary in order to more exactly locate the position of the $6A_1 \rightarrow 4T_{1g}$ absorption. This absorption feacture is commonly quite broad (See figure 5), and it is difficult to accurately locate its minimum visually. By converting to a digital format, the wavelength position could be located mathematically. The strip charts were taped to the board and the digitizing was done in the point, rather than the stream, mode. The corners of each spectrum representing 800 nm/100%R, 800nm/0%R, and 1200 nm/0%R, were digitized first to register the spectrum to the digitizing board. A minimum of 80 points along each spectral curve were then digitized. A high concentration of points near the bottom of the reflectance curves were digitized. Fewer points along the wings of the absorption features were digitized. Each spectrum was digitized six times. The first derivative of the digital data was calculated through a program written by Kenneth Nellis, Science Management Corporation, to locate the center of the ferric absorption feature. The high and low value of the center point was discarded and the average of the four remaining values was reported.

Surface Milling

After the optical depth experiments, it was found that only the top 50 μm of a typical rock coating contributed to the rock's visible-near IR reflectance spectrum. It was necessary to analyze only the top 50 μm in order to examine mineralogical constituents which contribute to the rock's reflectance spectrum.

A Powermatic Millrite industrial milling machine was utilized to remove the coating. A stainless steel 1/4 inch bit turning at 75 rpm's was employed. Each rock sample was mounted in the sample vise on the machine. The turning bit was lowered until it touched the sample, and was locked in position. The sample vise was raised 50 μm and then lowered. This process was repeated until enough sample was ground off for mineralogical analysis. The accuracy of the milling operation was approximately $\pm$ 20 μm. Some samples, such as coarse grained granodiorites, crumbled, and an accurate milling could not be completed.

Mineralogy of Natural Samples - Sample Preparation for X-Ray Diffraction - Soils

In the sampling areas utilized for this study, 10 - 100% of any particular sampling site was soil cover. The contribution of soil minerals to the overall reflectance spectrum on a site was, therefore, variable. The majority of the techniques used to prepare samples for x-ray diffraction are taken from Jackson (1974).

A size fractionation was necessary for clay mineralogic analysis. By concentrating the clay minerals and removing all coatings, preferred orientation of the clay platelets was possible. The first step in the size fractionation was the removal of soluble salts to aid in dispersion. This was accomplished by washing and heating 10 gram aliquots of the soil samples in 75°C pH5 1N NaOAc. Next, organic matter was removed by the addition of 30% H_2O_2.

Iron oxides commonly cement the clay minerals together. However, iron oxides were important in this study since they produce a major absorption feature in the visible-near IR spectrum. In order to mineralogically analyze the soil clay minerals, the iron oxides were removed by the Dithionite-Citrate-Bicarbonate (DCB) extraction. The soil was added to 70 ml of Na-citrate/Na-bicarbonate/NaCl complexing and buffering solution, and heated to 75°C. Two grams of Na-dithionite, a reducing agent, was added to the solution. The ferric iron was reduced to ferrous and complexed in solution. The liquid was decanted and saved for iron elemental analysis.

Using Stokes' law, the soil samples were separated into the less than 2.0 μm, 0.2 - 2.0 μm, 2.0 - 5.0 μm, and greater than 5.0 μm partical size ranges. The sized samples were dried and weighed to measure the size distributions. Two 60 mg aliquots of each size range were withdrawn, one was saturated with K^{+1}, and the other with Mg^{+2}. The Mg^{+2} saturated samples were glycérol solvated. Each sample was pipet-

ted onto a glass slide and allowed to dry in a sealed drying cabinet to avoid airborne dust and to allow for controlled drying conditions.

Sample Preparation for X-Ray Diffraction - Rock Coatings

The milled rock surfaces underwent a minimal amount of x-ray diffraction preparation. They were reground in a tungsten carbide mortar and pestle until the samples would pass through a number 400 sieve (44 μm hole size). A portion of the sample was then mounted with acetone on a glass slide. Analysis for x-ray diffraction was then conducted on a Siemens diffractometer with Cu K_a radiation. A graphite monochrometer was employed to reduce background noise. The scans were collected from 40° to 2° 2θ at a scan rate of 1° 2θ/min.

Following analysis of the samples by other methods, the samples were size fractionated to collect only the less than 2.0 μm fraction. This portion was weighed and assumed to be entirely clay minerals. This assumption was verifed by re-x-raying the less than 2.0 μm fractions and examining the scans for diffraction peaks identifiable as other than clay minerals. The less than 2.0 μm weight fraction was used in later calculations as the sample fraction responsible for the 2200 nm visible-near IR reflectance signal on the rock samples.

Mossbauer Spectroscopy

A Mossbauer spectrum was collected for selected rock coatings. A weighed sample was mounted in a plastic sample holder and placed in a brass sample block mounted on a liquid N_2 cryostat. Enough sample was included to reduce the total count rate reaching the detector to 1/3 of its initial count rate. All samples were initially run at liquid N_2 temperatures. A NaI detector was utilized and the absorption and velocity data were collected by a 400 channel multichannel analyzer. Synthetic hematite, enriched in ^{57}Fe, and iron foil was periodically rerun to check for electronic drift. A 50 mCi Co/Rh source was used. The Lorentzian fitting was completed using the MOSE program, on file with Dr. Leopold May, Catholic University of America, Washington, D.C. The MOSE program allows each Lorentzian peak to be fit individually. Other Mossbauer programs, such as MOSFIT, place constrictions on the fitting. MOSFIT, for instance, forces the fit to produce peaks in an ideal 3 - 2 - 1 - 1 - 2 - 3 peak area relationship. Another constraint forces the fitting of the inner two peaks first. This initial fitting constrains the position of the next two peaks. The fitting of these first four peaks constrains the placement of the outer two peaks. Since this study was concerned with identifying the ferric mineralogy through the position of the outer two peaks, these constrictions were not necessary. The MOSFIT program was tried on the initial

Mossbauer data set and found to cause inaccurate fits of the outer two peaks.

Resonant absorbtion data was collected from +10 mm/sec to -10 mm/sec for a period of between 12 and 36 hours, depending on the iron content of the sample. Samples which were low in iron were concentrated by boiling in 5N NaOH. They were then rerun.

The hematite-rich samples were rerun at room temperature and the room terperature effective field measurement vs. aluminum content was derived.

Four synthetic goethite samples were utilized to calibrate effective field vs. mole % aluminum substitution. The preparation of the synthetic goethite is described in the preceding section. The mole % aluminum was derived from the shift in the (111) x-ray diffraction d spacing, as described by Golden (1979).

Reagent grade Fe_2O_3 and two natural soils containing aluminum substituted hematite were used to calibrate mole % aluminum vs. effective field for the room temperature spectra of hematite. The degree of aluminum substitution was derived from the shift in the (300) x-ray diffraction d spacing, as described by Schwertmann (1979).

Chemical Extractions

Another technique was utilized for ascertaining the mole % aluminum substitution in the iron oxides, the DCB extraction technique. The technique is described in the pre-

vious section on soil x-ray diffraction preparation. The technique was used on ground rock coatings as well as soils. It extracts aluminum incorporated in the iron oxides along with the iron oxides. A problem with the technique is the reported possibility that fine grained aluminum oxides are also attacked. This would cause an increase in the extracted aluminum content. Boiling the samples in 5N NaOH for one hour destroys aluminosilicates and does not harm the iron oxides (Norrish and Taylor, 1961). Using this as a pretreatment for the DCB extraction ensures that all of the aluminum in the extract had iron oxides as its source.

The liquid extracts from the DCB treatment was examined by DC plasma spectroscopy and x-ray fluorescence for aluminum and iron analysis.

EXPERIMENTAL RESULTS AND DISCUSSION

Optical Depth

The optical depth experiments were designed to indicate what portion of a natural rock sample contributes to features in the rock's visible-near IR reflectance spectrum. The synthetic samples were made to model natural rock coatings which are commonly mixtures of weathering products deposited by water. The composition of each sample suite is listed in table 2.

The result of this experiment was to measure the depth within a rock sample below which a mineral, which has a visible-near IR reflectance feature, would not appear in the sample's VNIR reflectance spectrum. This depth is the optical depth. The reflectance value R at the ferric charge transfer reflectance minimum was converted to the Kubelka-Munk (KM) function and plotted against sample thickness for each suite. The Kubelka-Munk function f(R), is a transformation of the reflectance value, R, where R is measured on a sample vs. the reflectance of a standard, such as MgO. The function is calculated:

$$f(R) = \frac{(1 - R)^2}{2R}$$

Figure 11 represents the goethite/kaolinite suites. The four suites in the figure represent 25%, 50%, 75% and 100% goethite by weight.. The remainder of each suite is

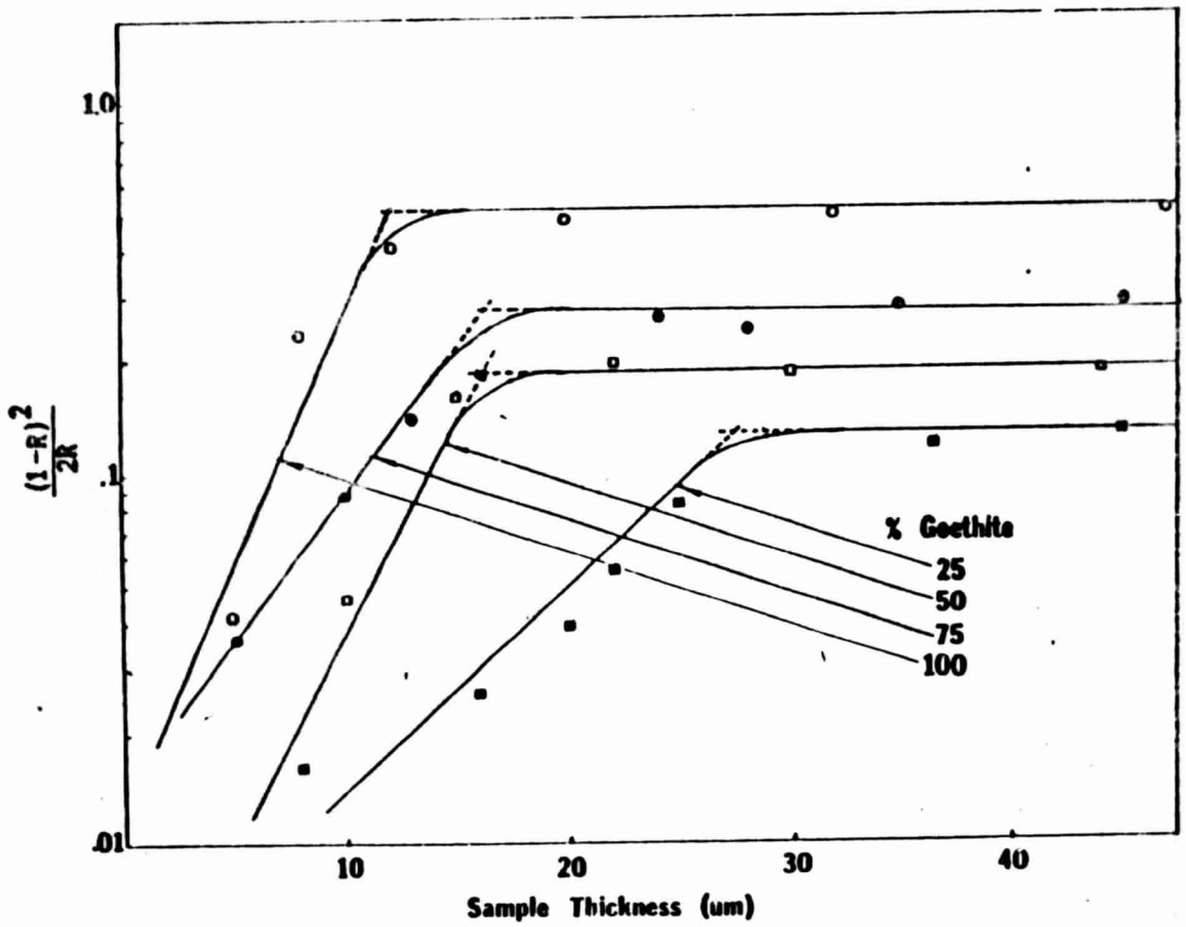

Figure 11. Relationship between sample thickness and absorption intensity of the $6A_1 \_\_ 4T_{1g}$ crystal field transition for goethite bearing samples. The weight % goethite is indicated.

kaolinite. The vertical axis is plotted as the Kubelka-Munk function, f(R), where R is the reflectance of the sample at the 900 nm minimum compared to the reflectance of $BaSO_4$. The reflectance of $BaSO_4$ is nearly 100% at this wavelength. A decrease in R causes an increase in f(R), therefore a high f(R) value indicates a low reflectance value. Within one suite, for instance, the 75% goethite suite, an increase in sample thickness results in an increase in f(R) (see figure 12). This trend continues until a saturation point is reached. This point is the suite's optical depth. Any increase in thickness beyond the optical depth does not result in an increase in f(R). It can therefore be concluded that any absorbing species occurring in the sample below the optical depth does not contribute to the sample's reflectance spectrum.

The optical depth appears to be related to the concentration of the absorbing species. In samples containing 100% goethite, the optical depth is approximately 10 μm. The optical depth increases to 28 μm for samples containing only 25% goethite. Kaolinite, the other constituent in these samples, is essentially a 100% reflector at this wavelength. As kaolinite's concentration increases and goethite's decreases, the incident radiation is scattered deeper into the sample before being absorbed.

The second feature of note is the value of the maximum f(R) for each suite. f(R) is the highest for the saturated 100% goethite sample suite and lowest for the 25% goethite

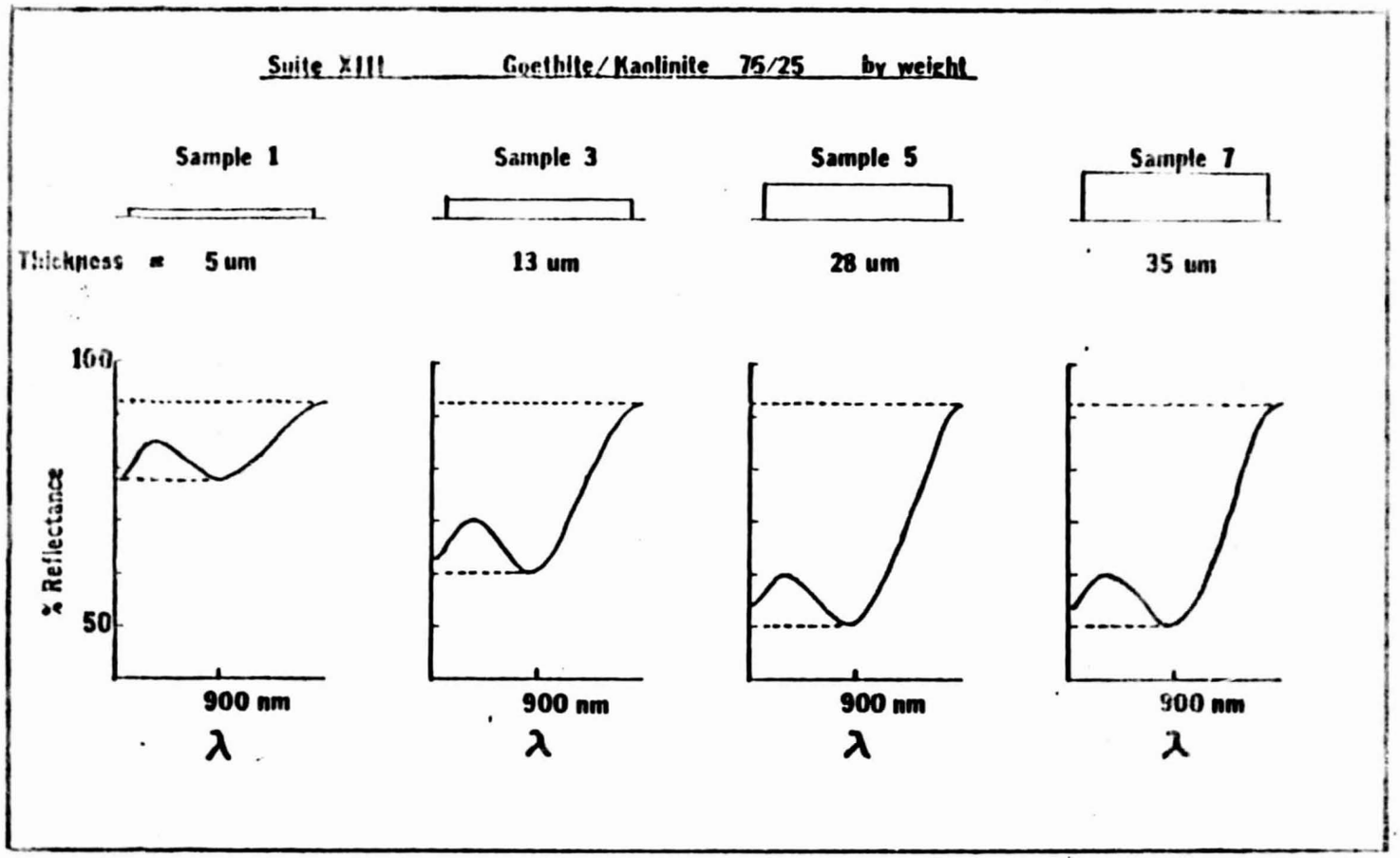

Figure 12. Representation of the effect of increased sample thickness on the absorption intensity of the $6A_1 \rightarrow 4T_{1g}$ crystal field transition which occurs near 900 nm.

suite. This indicates that f(R) is somewhat sensitive to the concentration of the absorbing species in infinitely thick samples. These suites all were of the same particle size and their packing density should have been approximately the same. This change in f(R) with concentration may prove of interest in later studies.

Figure 13 shows the same relationship for the hematite/kaolinite suites. In this case, the optical depth varies from approximately 13 μm to 20 μm. The change in f(R) with concentration is not as well resolved for the hematite bearing suites. The f(R) value for the high concentration suites is essentially the same. Since hematite contains more iron than goethite, the upper concentration suites may have been beyond any linear portion of the concentration-f(R) curve. Figure 14 shows the same relationship for aluminum subsitituted goethite/halloysite. The optical depth varies from 27 μm to 30 μm for the 25% and 50% aluminum substituted goethite suites. These samples have an even lower concentration of iron than the goethite suites. Their higher optical depth is probably a result of this lower iron concentration.

Several suites were made by mixing other clays besides kaolinite with hematite and goethite. The other clays used were halloysite and montmorillonite. No significant change in the data was produced by the substitution of different clays. This would be expected since both clays are nearly 100% reflectors at 900 nm.

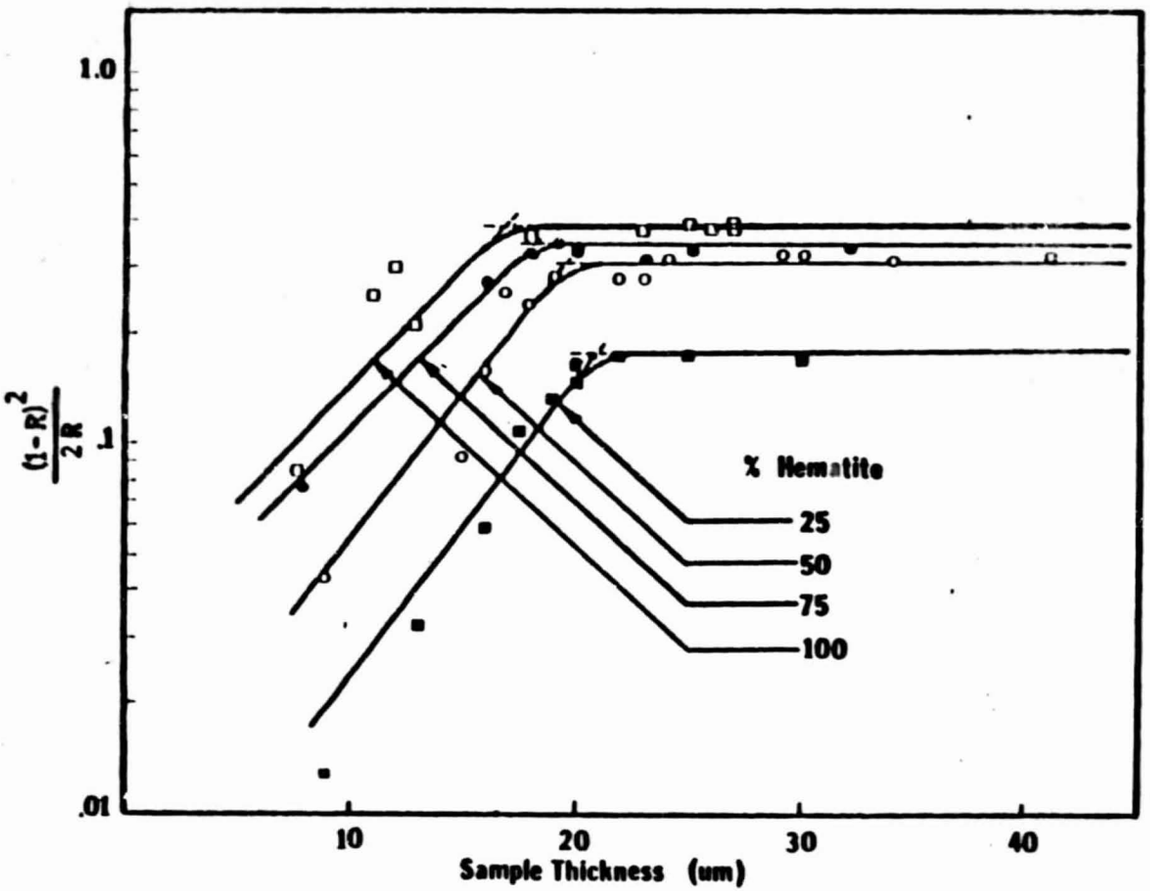

Figure 13. Relationship between sample thickness and absorption intensity of the $6A_1 - 4T_{1g}$ crystal field transition for hematite bearing samples.

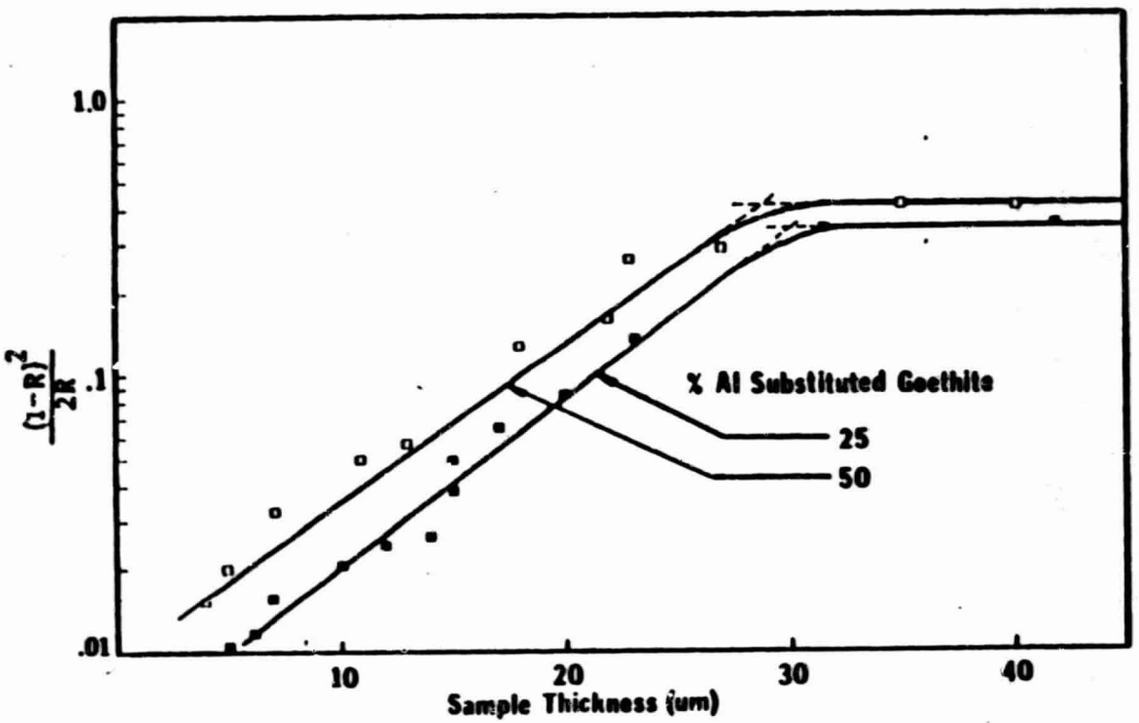

Figure 14. Relationship between sample thickness and absorption intensity of the $6A_{1g} \rightarrow 4T_{1g}$ crystal field transition for Al substituted goethite bearing samples. The weight % goethite is indicated.

The samples plotted in figures 11, 13, and 14, contain minerals whose particle size was between 0.2 µm and 2.0 µm. Several suites were used with size fractions less than 0.2 µm, and 2.0 - 5.0 µm. Again, no significant change in the data was produced.

A suite of 100% kaolinite samples was analyzed by the same method, except the 2200 nm feature produced by the fundamental hydrozyl stretch and the Al-OH bending mode was measured. The intensity of this reflectance minimum was converted to f(R) for each sample and plotted vs. sample thickness. The optical depth of this suite was 44 µm indicating that kaolinite residing at a greater depth from a sample's surface will contribute to the sample's reflectance spectrum.

The results of this experiment indicate that the uppermost 40 - 50 µm of a rock surface contributes to the sample's reflectance spectrum. If a mineralogical analysis is to be integrated with a reflectance spectrum, only the top 50 µm should be analyzed.

Since rocks are heterogenous, this sampling limitation is important. Several researchers have reported the limited thickness of other types of superficial rock coatings (Engle and Sharp, 1958; Potter and Rossman, 1977; Allen, 1978). The coatings in these cases were mineralogically distinct from the underlying rock (Potter and Rossman, 1979) and often have an external source. Since they are so thin, the inclusion of the unweathered underlying rock would cause the

mineralogy of the thin coating to be diluted in a mineralogical analysis.

Analysis of Thin Sections

Thin sections were made of 15 rock samples from both altered and unaltered sites. They were analyzed by both the electron microprobe and the SEM to note the occurrence of any enriched or leached zones within the weathered rock surface. Fe, Al, and S x-ray mapping and line scans were made to note the changing elemental concentrations vs. depth into the sample surfaces.

G6

The microprobe elemental maps appear in figure 15. The photographs show a general depletion of S in the outer surface. The XRD results show alunite to be the major sulfur bearing phase. Fe is enriched in the outer surface. The Fe phase is hematite and Mossbauer spectroscopy indicates it is essentially Al free. Al (15b) appears constant throughout the sample. Away from the sample surface it presumably occurs in alunite. Near the surface Al does not occur in alunite since S is depleted in this zone. Al probably occurs as a clay mineral or oxide. Its source can only be inferred since XRD and VNIR reflectance results do not identify its source.

SE micrographs were made of this same sample but at a different location (Figure 16). In these photographs, line

a.

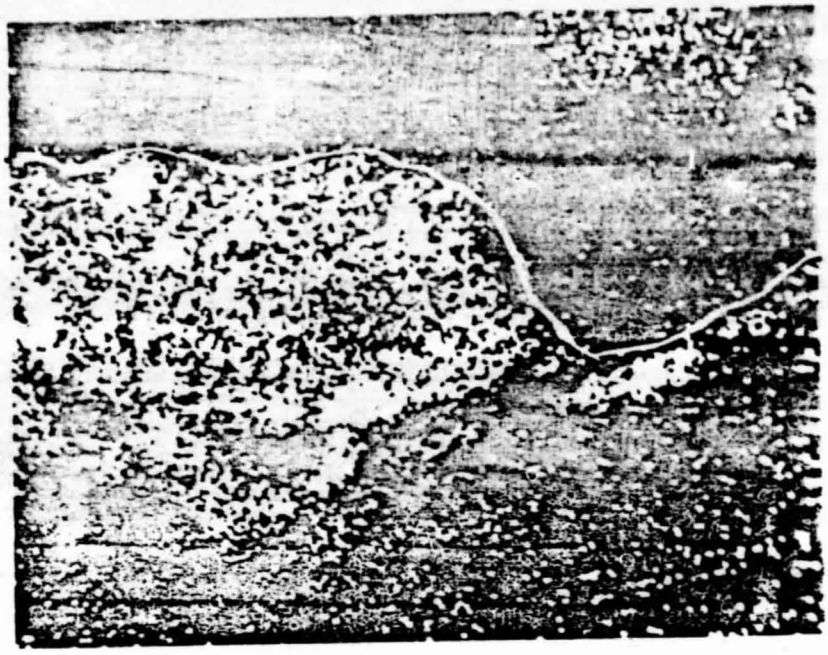

Figure 15. Elemental x-ray maps of the cross sectional thin section cut from sample 3f. White areas indicate high concentration. a. Iron map. b. Al map. c. Si map.

c.

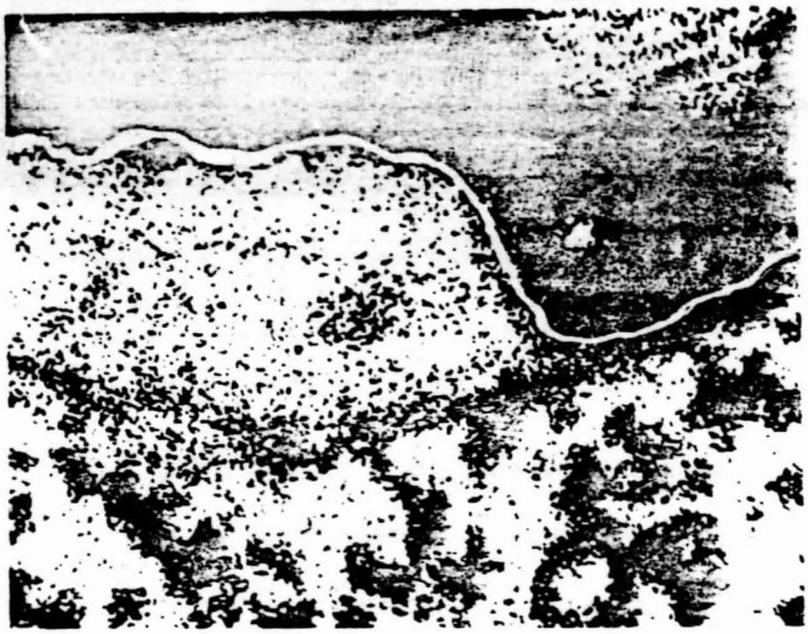

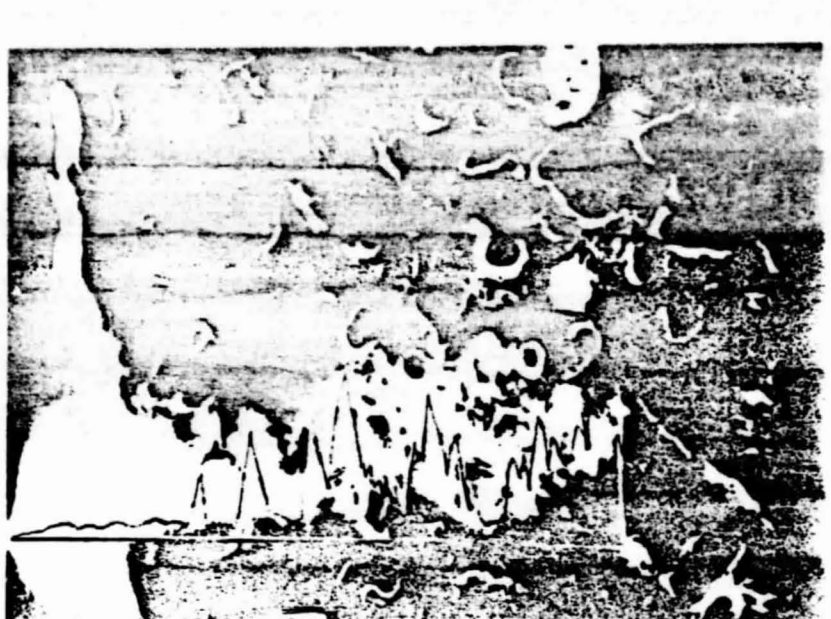

Figure 16. X-ray line scans of the cross sectional thin section cut from sample 36. a = Si; b = Al; c = Fe.

ORIGINAL PAGE
BLACK AND WHITE PHOTOGRAPH

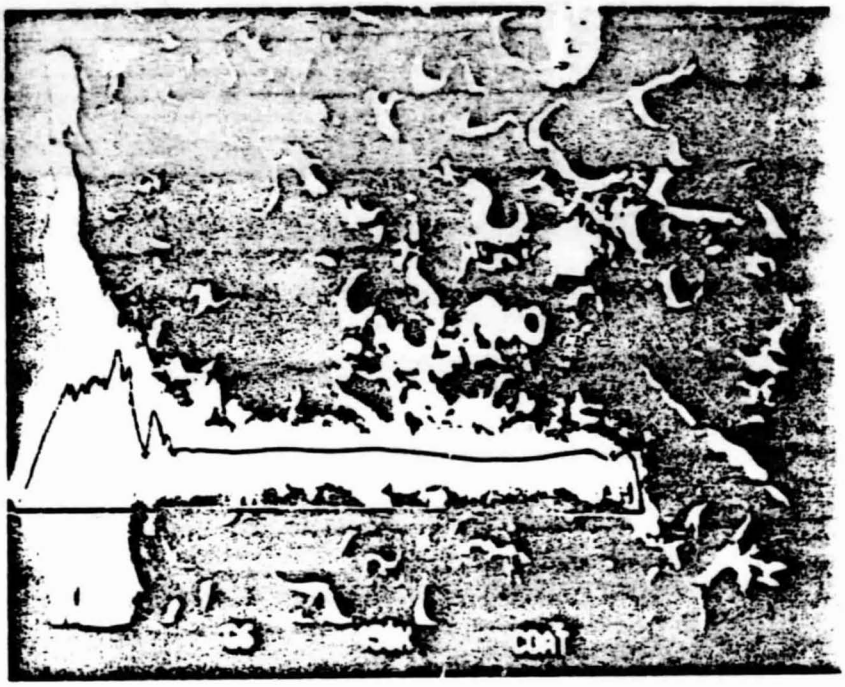

scans were made for Al, Fe, and S. The results are essentially the same as the microprobe results. S is depleted on the surface, Al is constant, and Fe is enriched on the surface. The depth of the Fe enriched/S depleted zone can be measured. It is approximately 40 µm. This indicates the composition of the top 40 µm is different than the underlying unweathered rock. The upper surface is depleted in alunite and enriched in hematite.

G8C

G8C was an altered dacite from Goldfield. Al and Fe x-ray maps were made of the thin section. Figure 17 shows Al concentration is rather constant throughout the entire cross section. The source of the Al is smectite, as indicated from the XRD results. The Fe is concentrated near the sample's surface. The iron occurs in Al free goethite.

Coaldale 6A

This sample (figure 18) is an unaltered, iron stained rhyolite. Maps were made of iron and aluminum concentrations. These maps show no Fe or Al enriched zones. Both elements appear to be homogeneously distributed. This coincides with field observations of this rock unit. It was seen as being iron stained throughout its matrix rather than having an iron stained surface coating.

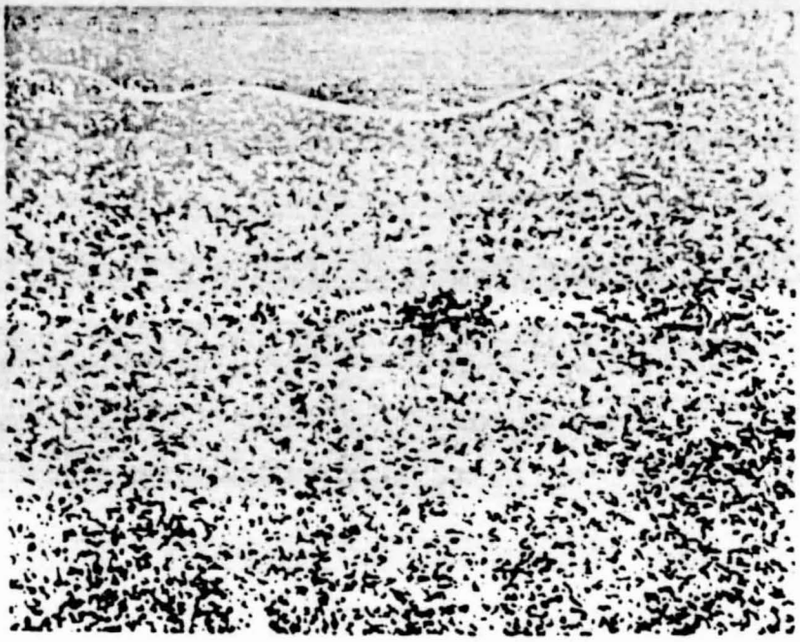

b.

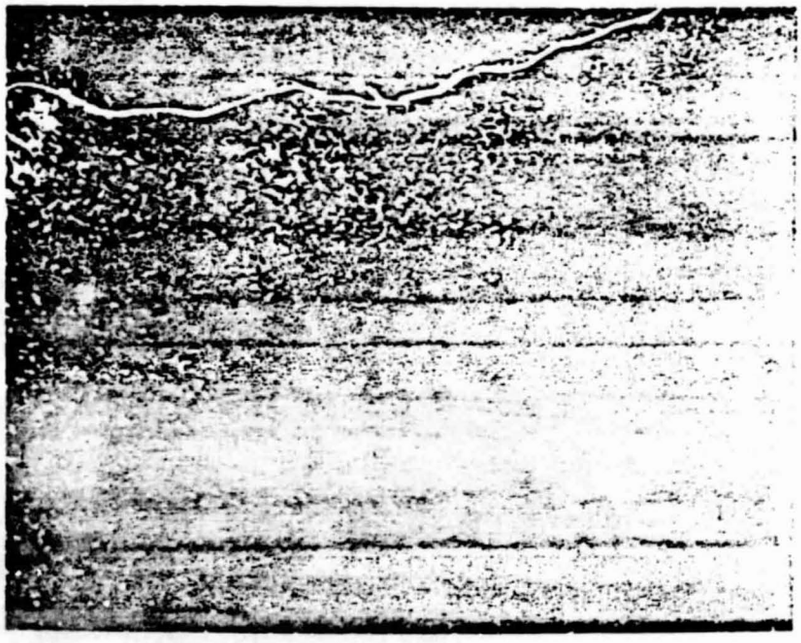

Figure 17. Elemental x-ray maps of the cross sectional - thin section cut from sample G8c. White areas indicate high concentration. a = Al; b = Fe.

a.

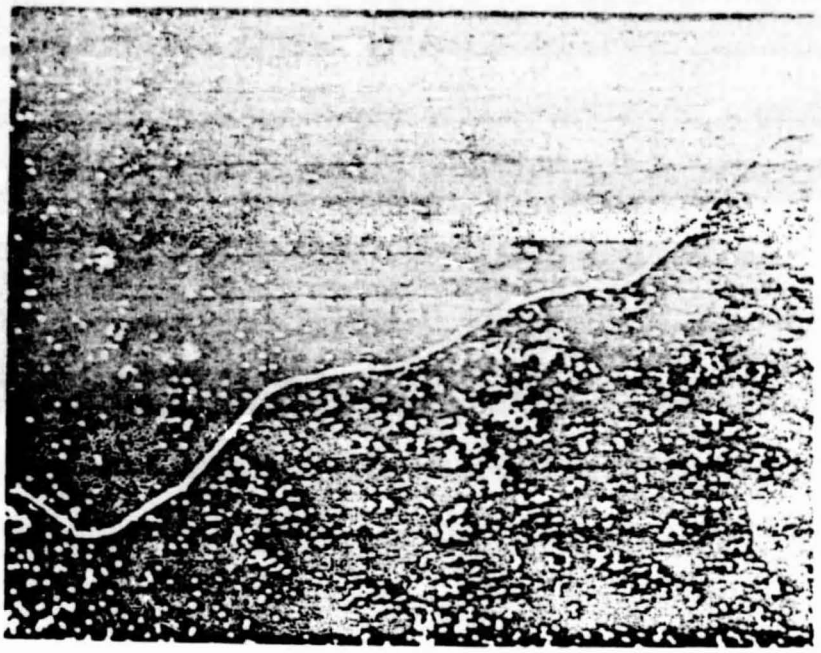

b.

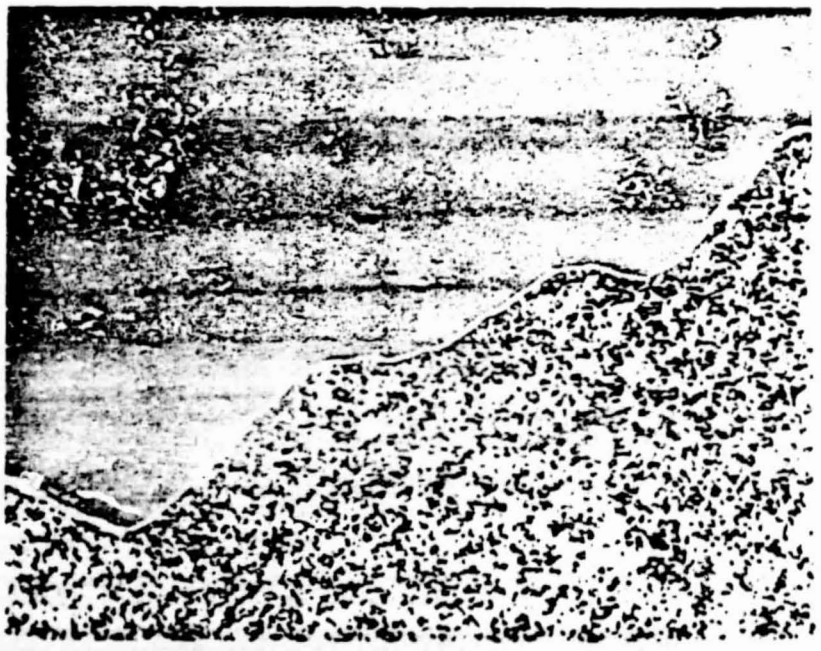

Figure 18. Elemental x-ray maps of the cross sectional thin section cut from sample Coaldale 6A. White areas indicate high concentration. A = Fe; B = Al.

Cand 36

This sample was an iron stained Paleozoic metasediment. The iron bearing phase, goethite, appeared to be depleted near its surface to a depth of approximately 20 µm. The calcite concentration, represented by calcium distribution, was variable. A depleted zone, also approximately 20 µm thick, occurred near the rock surface.

The results of these analyses support the need for analyzing only the upper surface when characterizing samples for remote sensing. Several samples showed surface zones in which minerals which contribute to a VNIR reflectance spectrum, such as calcite, alunite, hematite, or goethite, are depleted or enriched.

X-Ray Diffraction Mineralogy

XRD was the inital technique used for mineral identification of the top 50 µm of the rock samples. Table 4 is a key for the abbreviations used in all x-ray diffraction and visible-near IR mineralogical identifications. Tables 5 and 6 are compilations of the diffraction results for the altered and unalterd rocks.

There are inherent difficulties in attempting quantitative XRD. Changes in particle size and degree of crystalinity change the intensity of the diffraction peak. Individual minerals diffract x-rays with varying degrees of efficiency due to preferred orientation. There was no attempt

Table 4. Key for the abbreviations used in all x-ray diffraction and visible-near infrared mineralogical identifications.

Q = Qtz

F = Feldspar

H = Hematite

Mi = Mica

Cr = Cristobalite

Al = Alunite

Sm = Smectite

I = Illite

J = Jarosite

G = Geothite

K = Kaolinite

Ar = Aragonite

Ca = Calcite

Gy = Gypsum

Bi = Biotite

made in this study to derive quantitative information from the XRD patterns. The minerals are listed in terms of their relative percentages, with the first mineral listed being the most abundant and the last mineral the least.

One suite of samples was examined by other methods in order to quantify mineralogy. The mineralogy of this suite is listed in tables 5 and 7. The percent Fe and the percent S were measured by x-ray fluorescence. The percent clay was measured by size separation according to Stokes' settling law. The 2.0 μm size fraction is the clay size fraction. It was assumed for this study that only clay minerals occurred in this size fraction. The weight percent 2.0 μm. was assumed equal to the weight percent clay.

Goethite and hematite, two important minerals in remote sensing, were not positively identified by XRD. The minerals were apparent in the samples due to their characteristic color. They were not identified by XRD due to either their low abundance, their small particle size, or their disordered state.

Clay mineral identification is important in a remote sensing study since they are constituents which produce a recognizable feature in VNIR reflectance spectroscopy. The samples in this study were quite small, often less than 20 mg. This small sample size was unavoidable due to how the samples were produced. The upper 50 μm of rock surfaces were removed by milling. If the sample had a rough surface, as is the case with most tuffs, only a small sample could be

gathered in the milling operation. Due to the small sample size, many of the normal preparatory techniques for clay identification by XRD were not possible. Any clay with a room temperature peak at 10 A, which did not collapse with increased temperature, was identified as illite. This identification might include smectite, muscovite, or sericite. This study was to provide new criteria for remotely sensing hydrothermal deposits using the VNIR region. Since the above minerals have similar spectra in the 2200 nm region, their being grouped together should cause no difficulty.

The XRD results show that alunite and jarosite are found only in the altered areas. Since they are known as products of hydrothermal alteration, this is not surprising. They do not occur in all altered areas. When they occur, they are reliable indicators of hydrothermal alteration. Their non-occurrence does not indicate non-alteration.

The feldspar minerals only occur in unaltered rock. This is not surprising since the alteration of feldspar is a field identification of hydrothermal activity. One altered sample, G8 (Table 5), does include plagioclase. This is either a pre-alteration relic or was wind blown into the sample site. It is not an important point in the remote detection of ore bodies in the VNIR since feldspars have no signal in this region.

SiO_2, in several of its various phases, occurs in most of the samples. This silica has at least two sources, original rock material, and alteration products in silicified zones. This also is of limited importance since SiO_2 also has no absorption features in the VNIR.

As mentioned earlier, the clay minerals have intense absorption features in the VNIR due to overtones of AL-O-H bending and hydroxyl fundamental stretching. In general, clay minerals are present in the altered rocks and not in the unaltered rocks. This is not surprising since the areas sampled are all arid. Clay minerals are commonly produced through the chemical weathering of silicates. Arid conditions would slow the production of clays and cause low clay concentrations in unaltered rock. Altered rock has another source of clay minerals. The hydrothermal fluids break down feldspars and other silicates, and form clays in the alteration process. Some unaltered samples also contain clays, e.g. - Card and BR. These samples are of sedimentary origin. They contain clay minerals as rock forming constituents and not as weathering products. By observing only gross clay type, the clay minerals in the altered and unaltered samples cannot be differentiated. Dickite, for instance, has been reported as the form of kaolinite which is hydrothermally formed (Hurlbut, 1971). Clays were not classified according to polytype in this study. This would be an interesting area for future study.

Table 5. Mineralogy of the upper 50 μm of rock sample collected along 1980 SMIRR flight lines.

Sample	Wt % Clay	XRD	VNIR	Altered or Unaltered
CD6	9.6	F,Q,H	---	U
CD7	9.0	F,Q,H	---	U
CD8	9.6	F,Q,H	---	U
LM3	5.3	Q,F,Mi	Mi,G/H	U
CP1	14.1	Q	K	A
CP3	7.0	Q	___	A
CP4	18.1	Cr,Al	A, K	A
CP9	---	Cr,Al	A, G/H	A
G4	22.8	Q,F,Mi	---	U
G6	6.8	Al,Q	A, G, H	A
G8	15.6	Sm,F,Q	M, G, H	A
EX2	44.9	Sm,Cr	M	A
CC1	---	Q,I,J	I, J	A
CC2	10.0	J,Q,K	K, J	A
Cand	---	---	C, G	U

Table 6. Mineralogy of the upper 50 μm of rock samples collected in 1979 from hydrothermally altered and unaltered rock units.

Sample	XRD	VNIR	Altered or Unaltered
CC1	I	I	A
CC2	Q, J, I	I	A
CC3	Q, K, I	G, K	A
CC4	Q, I	A, K	A
CC5	Q, I	I, G/H	A
CC6	Q, J, I	J, I, G/H	A
CC7	Q, J, I	J, I	A
CC8	Q, K	K, G	A
CC9	Q, K	---	A
CC10	Q, J, I	J	A
CC11	Q, J, I	---	A
RH1	Q, 2F	I	U
RH2	Q, 2F	I	U
RH3	Q, 2F	I	U
RH4	Q, 2F	I	U
G1	Q, J	---	A
G1arg	Q, J	J, G	A
G2sil	Q, J	J, G	A
G3	Q, Al	---	A
G4	Q, Al, J	---	A
G5	Q, K	---	A

Tunell, G., Posnjak, E.; Stability Relations of Goethite and Hematite; Economic Geology, 26, 337-343. 1931.

Vincent, R.K., Hunt, G.R.; Infrared Reflectance From Mat Surfaces; Applied Optics, 7, (1), 1968.

Wang, M.K.; Formation of Goethite and Hematite at 70 °C; Ph.D. Dissertation, Rutgers University, The State University of New Jersey - New Brunswick, 1978.

Watson, K.; Regional Thermal-Inertia Mapping to Discriminate Geologic Materials; Summaries of the 13th International Symposium on Remote Sensing, Ann Arbor, 1979.

Wendlandt, G.R., Hecht, R.H.; Reflectance Spectroscopy, McGraw-Hill, New York, 1971.

C-3